

# Zero-Knowledge Location Privacy via Accurate Floating Point SNARKs

Jens Ernstberger\*  
jens.ernstberger@tum.de  
Technical University of Munich  
Munich, Germany

Chengru Zhang\*  
u3008875@connect.hku.hk  
The University of Hong Kong  
Hong Kong, Hong Kong

Luca Ciprian  
luca.ciprian@tum.de  
Technical University of Munich  
Munich, Germany

Philipp Jovanovic  
p.jovanovic@ucl.ac.uk  
University College London  
London, United Kingdom

Sebastian Steinhorst  
sebastian.steinhorst@tum.de  
Technical University of Munich  
Munich, Germany

## ABSTRACT

This paper introduces Zero-Knowledge Location Privacy (ZKLP), enabling users to prove to third parties that they are within a specified geographical region while not disclosing their exact location. ZKLP supports varying levels of granularity, allowing for customization depending on the use case. To realize ZKLP, we introduce the first set of Zero-Knowledge Proof (ZKP) circuits that are fully compliant to the IEEE 754 standard for floating-point arithmetic.

Our results demonstrate that our floating point implementation scales efficiently, requiring only 69 constraints per multiplication for  $2^{15}$  single-precision floating-point multiplications. We utilize our floating point implementation to realize the ZKLP paradigm. In comparison to the state-of-the-art, we find that our optimized implementation has  $14.1\times$  less constraints utilizing single precision floating-point values, and  $11.2\times$  less constraints when utilizing double precision floating-point values. We demonstrate the practicability of ZKLP by building a protocol for *privacy preserving peer-to-peer proximity testing* – Alice can test if she is close to Bob by receiving a single message, without either party revealing any other information about their location. In such a configuration, Bob can create a proof of (non-)proximity in 0.27 s, whereas Alice can verify her distance to about 250 peers per second.

## 1 INTRODUCTION

Location-based services are ubiquitous in the current era of digital connectivity. The proliferation of devices capable of precise geolocation tracking, such as smartphones and connected vehicles, has fueled advancements in services reliant on spatial data. For example, OpenStreetMap [39], a map project generated from user-contributed GPS data, reports 10.6 million registered users as of January 2024 [40]. However, these developments also raise significant privacy concerns, as location data can reveal sensitive information about an individual’s habits and preferences. A tracking adversary, such as the network operator or intended service provider, may easily monitor public Global Navigation Satellite System (GNSS) signals [28, 63], and insurance policies may demand for centralized data aggregation to tailor policies based on individual driving habits and locations frequented [35].

In response, numerous Location Privacy Preserving Mechanisms (LPPM) protocols emerged to protect user location privacy [10, 29].

These solutions either rely on obfuscation [1, 34], which aims to reduce the precision of location-based information, or cryptography [32, 41, 36, 49], which utilizes secure computing and encryption rather than distortion to ensure privacy protection. Unfortunately, either solution introduces shortcomings. LPPM utilizing differential privacy does not perform well for location information that is correlated between users [38]. Other obfuscation mechanisms based on cloaking [34], as well as cryptographic mechanisms based on multi-party computation [49], are reliant on a third party for data anonymization. An ideal mechanism protects personalized location information without relying on third-party communication, and ensures strong geo-indistinguishability.

This paper initiates research on *ZKLP*. Our approach is driven by recent advancements in Zero-Knowledge Proofs (ZKPs), which enable practical use in applications previously deemed too costly. With ZKLP, users can prove to any third party that they are within a specific geographical region, whilst obfuscating their exact location for utility and privacy. Third parties only obtain an obfuscated location, whose correctness can be verified in milliseconds. To do so, we rely on Discrete Global Grid Systems (DGGS) with hexagons as geometric representation, which divide the Earth into a hierarchy of progressively finer resolution grids. We demonstrate the practicability of our new paradigm by developing a protocol for privacy-preserving peer-to-peer proximity testing.

**Importance of Floating-Point for ZKLP.** Location information usually consists of fractional numbers, which are represented as either fixed-point or floating-point numbers in computer software and hardware. However, ZKPs often require the statement to be encoded as an arithmetic circuit, while it is challenging to represent these values accurately in-circuit. Although it is common practice to use fixed-point numbers in-circuit [30, 31], this is suboptimal for ZKLP. Looking ahead, in DGGS, we need to handle large values (e.g.,  $\sqrt{7}^{\text{res}}$  where  $\text{res}$  is the hexagonal resolution) and small values (e.g., the product of  $\sin \theta$  and  $\cos \theta$ ) simultaneously, resulting in either increased data size or reduced accuracy in fixed-point representation. Therefore, we introduce optimized circuits for primitive floating-point operations, compliant with the IEEE 754 floating-point standard [27]. We deem this contribution of independent interest as in modern computer hardware, real numbers are represented as floating-point values as a default format. Previous works have investigated the use of floating-point values in ZKPs, targeting verifiable inference and training of machine learning models [56,

\*Both authors contributed equally to this research.

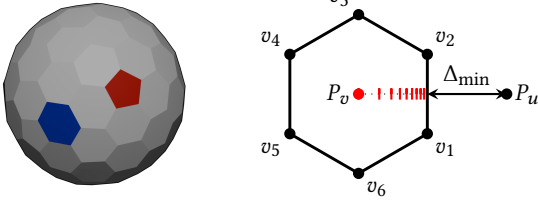


**Figure 1:** (i) **Icosahedral Polyhedron.** A hexagon is highlighted in blue, and a pentagon is highlighted in red. (ii) **Hexagon**  $h = [v_0, v_1, \dots, v_6]$ .  $P_u$  and  $P_v$  denote the points of user  $u$  and  $v$  respectively. In ZKLP,  $v$  is the prover and  $u$  is the verifier.  $\Delta_{min}$  is the privacy-preserving distance of  $u$  to  $v$ . The red ticks depict our methodology to evaluate ZKLP in Section 5.

20, 19]. However, they are either (i) not optimized for Succinct Non-Interactive Arguments of Knowledge (SNARKs) or (ii) not fully compliant with the IEEE standard. Note that even though our ZKP circuits can provide full IEEE 754 compliance, the ZKLP paradigm does not require a strong compliance with the IEEE standard, which allows us to further lower the SNARK size by disabling the logic for handling edge cases, like NaN and  $\pm\infty$ .

**Challenges for Floating-Point.** Efficiently emulating floating-point operations in a SNARK is hard. A SNARK commonly operates over a finite field  $\mathbb{F}_p$ , where  $p$  is a large prime depending on the underlying elliptic curve (e.g.,  $|p| = 254$  for BN254). By contrast, 32- or 64-bit floating-point numbers require integer operations that are circuit-unfriendly, such as comparison and shifts. A naive in-circuit implementation for floating-point representation and operations would lead to a huge number of constraints [3, 56, 20]. Garg et al. [20] address this problem by proving the upper bound of the relative error, instead of transforming floating-point operations to in-circuit bitwise operations. In spite of this, their work only supports addition and multiplication. To realize ZKLP, we require complex operations such as division, taking square roots, and trigonometric functions. In addition, we also need to guarantee that these operations produce correctly rounded results, which introduces more constraints. Hence, emulating floating-point numbers precisely, whilst attaining efficiency in the operations involved, is costly without significant optimization.

**Challenges for ZKLP.** Transforming a location described as latitude and longitude to an index in a hexagonal grid system requires extensive use of trigonometric operations. Common approaches to approximating trigonometric functions by following the standard three-step recipe of *range reduction*, *polynomial approximation*, and *output compensation*, rely on high bitwidths to obtain precise results [45]. Further, naive polynomial approximation through, e.g., Taylor Series, is prohibitively expensive in-circuit, as precise results demand for many iterations, which is expensive to represent in an arithmetic circuit that demands for linearization.

## Contributions & Results

We provide a full implementation of IEEE 754 compliant floating-point operations in SNARKs and apply them in our implementation of the ZKLP paradigm. To demonstrate the power of ZKLP, we

implement *privacy-preserving peer-to-peer proximity testing*, which evaluates the minimal distance to a peer without forfeiting privacy.

The main technical contributions of our work are (i) novel optimizations for computing floating-point SNARKs and (ii) optimizations to eliminate trigonometric operations that make the ZKLP paradigm practical. Throughout, we leverage lookup arguments and nondeterministic programming, enabling cost-effective representation of computations that are typically resource-intensive when executed in-circuit. To efficiently operate on floating-point values, we convert their integer components to an equivalent but circuit-efficient form, build optimized sub-circuits for integer operations, and minimize the number of costly range checks in key steps, e.g., rounding. For compliance with IEEE 754, we take additional care of edge cases, such as NaN,  $\pm\infty$  and subnormal numbers. To efficiently instantiate ZKLP over primitive floating-point operations, we introduce shortcuts, eliminating expensive math operations through trigonometric identities and nondeterministic programming.

Our experiments show that our circuits for primitive floating-point operations are precise and performant. We test our implementation with the Berkeley TestFloat library [26] to ensure full compliance. The extensive use of lookups leads to amortization —  $2^1$  FP32 multiplications require 214 constraints, whereas  $2^{15}$  FP32 multiplications require 69 constraints per operation. When applied to the ZKLP paradigm, our resulting circuits are highly efficient. In comparison to a fixed-point baseline without optimizations, our implementation has  $14.1\times$  less constraints utilizing single precision floating-point values, and  $11.2\times$  less constraints when utilizing double precision floating-point values. When applied to privacy-preserving peer-to-peer proximity testing, we show that a user can evaluate its proximity to about 250 peers per second.

In summary, our contributions are as follows:

- **ZKLP.** We introduce ZKLP, a novel application of ZKPs, along with a full implementation and evaluation. ZKLP unlocks a novel class of ZKP-empowered applications, which enable personalized location privacy through geo-indistinguishability. In particular, it allows individuals to prove that they have visited a certain location whilst ensuring privacy for the exact location.
- **IEEE 754 Compliant Floating-Point SNARKs.** We introduce optimized SNARK circuits for floating-point operations that are fully compliant to IEEE 754 [27] and fulfill its precision requirements in Section 3. Our optimization for primitive floating-point operations are universally applicable, and we therefore consider them of independent interest.
- **Optimizations for ZKLP.** Transformations on geographic coordinates demand for extensive use of trigonometric functions. In Section 4, we introduce optimized ZKP circuits that avoid and eliminate trigonometric functions for ZKLP.
- **Evaluation & Application.** In Section 5, we evaluate our floating-point circuits and showcase the capabilities of ZKLP by applying it to peer-to-peer proximity testing.

## 2 PRELIMINARIES

### 2.1 Notation

We denote the bitwidth of an integer  $x \in \mathbb{Z}$  as  $|x|$ , and the concatenation of  $x, y \in \mathbb{Z}$  as  $x \parallel y$ . When we want to indicate the absolute value of  $x \in \mathbb{Z}$ , we write  $\text{abs}(x)$ . We use  $x \ll n$  and  $x \gg n$  to denote the left shift and the right shift operation on  $x$  by  $n$  bits, respectively, and we assume that the left shift operation does not move any bits out, i.e., all bits of  $x$  are preserved in  $x \ll n$ . For  $x, y \in \mathbb{Z}$  with  $y$ 's upper bound known to be  $Y$ ,  $\overline{x \parallel y}$  is a shorthand for  $\frac{x \parallel y}{Y}$ , where the division is done over rational numbers.

We define the position of a point on the Earth's surface in spacial coordinates by radial distance ( $r$ ), latitude ( $\theta$ ), and longitude ( $\phi$ ). Here,  $r$  approximates the Earth's radius,  $\theta$  represents the latitude, ranging from  $-90^\circ$  at the South Pole to  $+90^\circ$  at the North Pole with  $0^\circ$  at the Equator, and  $\phi$  represents the longitude, ranging from  $-180^\circ$  to  $+180^\circ$  with  $0^\circ$  at the Prime Meridian. We represent a vertex of a hexagon in two-dimensional Cartesian coordinates as  $v_i = (x_i, y_i)$ . We denote a hexagon as a vector in lower-case bold symbols, i.e.,  $\mathbf{h} = [v_0, v_1, \dots, v_i]$  where  $i \in \{0, 6\}$ . Let  $\mathcal{H} = \{\mathbf{h}_1, \mathbf{h}_2, \dots, \mathbf{h}_n\}$  be a set of regular hexagons in the Euclidean plane, each hexagon  $\mathbf{h}_i$  having a center point  $c_i$  and equal side length  $a$ . For each hexagon  $\mathbf{h}_i$ , there exists a region  $R_i$  in the plane, defined by the vertices of  $\mathbf{h}_i$ , with the property that every point within  $R_i$  is closer to  $c_i$  than to the center point of any other hexagon in the set  $\mathcal{H}$ . The region  $R_i$  is referred to as a *hexagonal cell*.

### 2.2 Background On Floating-Point Numbers

Fixed-point and floating-point are common methods for representing a real number in computers. In fixed-point representation, we fix a scaling factor  $N$  and represent a number  $x$  as an integer  $v$  of bitwidth  $M$ , whose lowest  $N$  bits are treated as the fractional part with an implicit decimal point in front, i.e.,  $x = \sum_{i=-N}^{M-N-1} v_i \cdot 2^i = \frac{v}{2^N}$ . Arithmetic operations on fixed-point numbers are equivalent to directly operating on their underlying integers, and only a small overhead is required to keep the scaling factor unchanged. The main advantage of fixed-point is that it can be more efficient in computation and storage, especially on low-cost hardware that lacks native support for floating-point arithmetic. However, it can only handle numbers with similar orders of magnitude, and lacks precise representation of very large or very small numbers simultaneously.

Floating-point representation does not have a fixed scaling factor. It uses only a portion of the available bits (*mantissa*) to store the number, and the remaining bits (*exponent*) are reserved for dynamically tracking the scaling factor. When operating on floating-point numbers, the exponent and mantissa need to be correctly updated. While increasing cost, floating-point representation is more general than fixed-point representation, as it can represent very small and very large numbers with greater precision.

IEEE 754 [27] is the de facto standard for floating-point numbers and is widely adopted by modern hardware and software. It defines the encoding formats of floating-point numbers and a set of arithmetic operations on these numbers. A floating-point number in the IEEE 754 standard consists of three components, the sign  $s$ , the exponent  $e$ , and the mantissa (or significand)  $m$ . The *binary* encoding format encodes these components as a binary string  $s \parallel e \parallel m$ ,

where  $s, e, m$  have 1,  $E, M$  bit(s) respectively. In this paper, we are interested in the most popular binary encoding formats FP32 (a.k.a. single precision, or formally binary32) and FP64 (a.k.a. double precision, or formally binary64). For FP32,  $E = 8, M = 23$ , and for FP64,  $E = 11, M = 52$ . Here, we give a brief overview of binary encoding format and discuss arithmetic operations in Section 3.

The binary encoding format is capable of representing 5 types of values, namely, *signed zeros* ( $\pm 0$ ), *subnormal numbers*, *normal numbers*, *infinities* ( $\pm \infty$ ), and *"not a number" values* (NaNs). For the sake of convenience, we use *abnormal* to denote a number that is either  $\pm \infty$  or NaN. Below we list how the IEEE 754 specification maps the encoded value  $s \parallel e \parallel m$  to the real number  $\alpha$ .

- (i)  $e = 0, m = 0$  ( $\pm 0$ )  $\rightarrow \alpha = 0$  if  $s = 0$  and  $\alpha = -0$  if  $s = 1$ .
- (ii)  $e = 0, m \neq 0$  (subnormal)  $\rightarrow \alpha = (-1)^s \cdot 2^{-2^{E-1}+2} \cdot \overline{0.m}$ .
- (iii)  $e \in [1, 2^E - 2]$  (normal)  $\rightarrow \alpha = (-1)^s \cdot 2^{e-2^{E-1}+1} \cdot \overline{1.m}$ .

In this case,  $e$  is the *biased form* of the actual exponent with  $2^{E-1} - 1$  as the bias, and  $m$ , together with an implicit leading 1, describes the actual mantissa.

- (iv)  $e = 2^E - 1, m = 0$  ( $\pm \infty$ )  $\rightarrow \alpha = \infty$  if  $s = 0$  and  $\alpha = -\infty$  if  $s = 1$ .
- (v)  $e = 2^E - 1, m \neq 0$  (NaN)  $\rightarrow \alpha$  isn't a numeric value.

It is straightforward to see that the encoding allows storing a normal number that is in the range  $[2^{-2^{E-1}+2}, 2^{2^{E-1}-1})$  with  $(M+1)$ -bit precision and a subnormal number that is even smaller, i.e., in the range  $[2^{-2^{E-1}+2-M}, 2^{-2^{E-1}+2})$ , with lower precision.

### 2.3 Discrete Global Grid Systems

DGGS divides the Earth into a hierarchy of progressively finer resolution grids. A naive solution for dividing the Earth's surface is to apply a simple latitude-longitude grid. The Earth is divided into a grid based on lines of latitude and longitude, creating a series of rectangular cells that cover the entire globe. However, the drawback of such an encoding is that near the poles, the lines of longitude are in closer proximity than they are at the equator. While a latitude-longitude grid is a simple way to partition the Earth's surface, it lacks the uniformity, efficiency, and scalability of a DGGS [48], particularly for complex spatial analyses and global-scale applications.

**Hexagonal Hierarchical Geospatial Indexing.** A long line of research suggests that defining a DGGS primarily based on hexagonal tiles exhibits superior properties than DGGS based on other geometric shapes for algorithmic efficiency [48, 47]. This benefit is evident in practical tools, showing adoption of hexagonal DGGS in practice. Uber, for example, introduced the Hexagonal Hierarchical Spatial Index, a geospatial index that partitions the globe into hexagons for more accurate analysis of movement patterns [54]. The global grid system relies on a gnomonic projection centered on icosahedron faces. In the Uber H3 indexing system, hexagons are utilized to create a grid on each icosahedron face. The H3 indexing system supports differing granularity, with 16 resolutions. At the highest resolutions, 122 hexagons span the sphere of the earth, with 10 hexagons per icosahedron face. As hexagons cannot tile a icosahedron face, 12 pentagons are introduced at each of the icosahedron vertices to tile the full spherical projection. To gain some intuition, we refer to Figure 1 which depicts an Icosahedral Goldberg Polyhedron of hexagons and pentagons with 92 faces.

## 2.4 SNARKS

A zero-knowledge Succinct Non-Interactive Argument of Knowledge (zk-SNARK) [6] is a cryptographic protocol, where a prover  $\mathcal{P}$  convinces a verifier  $\mathcal{V}$  that a certain NP-statement is true, without disclosing any information besides the veracity of the statement. Common SNARKs target the problem of *circuit-satisfiability*, i.e., providing SNARKs for arbitrary NP-statements, represented as arithmetic circuits (R1CS [21], Plonkish [17], AIR [5]). Informally, a zk-SNARK for circuit satisfiability satisfies the following:

**Succinct:** The verification cost and the size of the proof are sublinear in the size of the circuit.

**Non-Interactive:** The prover  $\mathcal{P}$  can provide a proof that can be independently verified by anyone without further communication.

Beyond the above properties of a zk-SNARK, the security properties of a zk-SNARK can be informally described as follows:

**Perfect Completeness:** An honest  $\mathcal{P}$  can always convince  $\mathcal{V}$  of the correctness of a true statement.

**Knowledge Soundness:** A dishonest  $\mathcal{P}$  cannot convince  $\mathcal{V}$  of an invalid statement, except with negligible probability. Furthermore, an extractor can successfully extract the witness for a valid statement except with negligible probability.

**Zero-Knowledge:** The proof reveals nothing to  $\mathcal{V}$  besides the fact that  $\mathcal{P}$  knows an assignment that satisfies the circuit predicate.

The proof system is termed an *argument of knowledge* if knowledge soundness holds against a computationally bounded prover.

## 2.5 SNARK Optimizations

Recent years have shown significant advancements in optimizing SNARKs, both on a cryptographic level and in educated circuit construction. We introduce generic SNARK optimizations, applied at various points in our protocols in Section 3 and 4, in the following.

**Lookup Arguments.** Most SNARKs can efficiently represent computations that can be expressed as an arithmetic circuit. However, there are some non-arithmetic operations, such as range checks, XOR or logical AND operations, that are unfriendly to the circuit and cost more constraints. Lookup arguments aim to reduce the prover complexity for these non-arithmetic operations by simply checking that a *query* is contained in a *lookup table* [58]. They were first introduced by Bootle *et. al* [7], and optimized in several successive works [52, 25, 61, 43, 62, 16, 11]. In this work, we consider precomputed lookup tables, where we precompute all valid values of a function and then perform a lookup to check inclusion in the lookup table by the lookup argument based on logarithmic derivatives [25]. We denote a lookup table as  $\mathcal{T}$ , which contains a vector of entries  $\mathbf{t} := (t_1, t_2, \dots, t_n) \in \mathbb{F}^n$ , and  $\mathbf{f} := (f_1, f_2, \dots, f_m) \in \mathbb{F}^m$  represents the vector of queries. Note, that the lookup table may consist of  $w > 1$  columns, and in this case, each element in the queries and entries can again be represented as a vector (i.e.,  $f_i, t_i \in \mathbb{F}^w$ ).

**Nondeterministic Programming.** An in-circuit computation proves that the input data satisfies a given compliance predicate. The local input data can provide arbitrary *hints* (or nondeterministic advice [37]), which are not trusted to be correct, but whose verification is more efficient in-circuit than the emulation of the plain computation. Hints leverage the fact that certain calculations are hard to compute, but easy to verify in an arithmetic circuit.

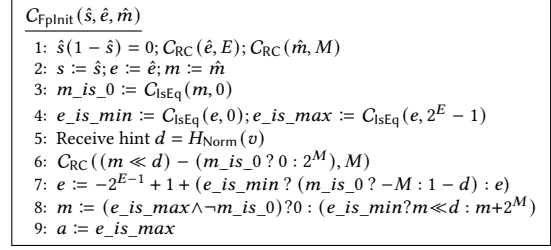


Figure 2: Circuit for initializing floating-point numbers

In consonance with related work [2], we formalize a *hint* as the computation  $H(X) \rightarrow Y$  done by the prover outside the arithmetic circuit. An in-circuit nondeterministic predicate  $P : X \times Y \rightarrow \{0, 1\}$  for  $H$  ensures that  $\forall x \in X, y \in Y$  the relations  $H(x) = y \iff P(x, y) = 1$  and  $H(x) \neq y \iff P(x, y) = 0$  hold. Note, that in practical applications, the variable returned by a hint function is equivalent to a prover-supplied witness. We call those variables hints instead of witnesses for separation of concerns, highlighting that the computation is done outside the circuit, and that their values are provided by the prover.

For example, consider extracting the most significant bit of the mantissa of a floating point value. Let the computation to find the MSB of a mantissa be  $H_{\text{MSB}}(m) = \text{MSB}_m$  and the nondeterminism predicate be  $P_{\text{MSB}} : \mathbb{Z}_p \times \mathbb{Z}_p \rightarrow \{0, 1\}$ . In the circuit, it is verified that  $\text{MSB}_m$  is indeed the MSB of  $m$  by the predicate  $P_{\text{MSB}}$ :

$$P_{\text{MSB}}(m, \text{MSB}_m) = \begin{cases} 1 & \text{if } m - \text{MSB}_m \cdot 2^{|\text{MSB}_m|-1} \in [0, 2^{m-1}], \\ 0 & \text{otherwise.} \end{cases}$$

If  $\text{MSB}_m = 0$  but the actual  $\text{MSB}_m$  is 1, then the expression  $m - \text{MSB}_m \cdot 2^{|\text{MSB}_m|-1}$  will result in at least  $|\text{MSB}_m|$  bits. If  $\text{MSB}_m = 1$  but the actual MSB is 0, the subtraction will result in a negative value.

## 3 PRIMITIVE FLOATING-POINT OPERATIONS

In the following, we introduce optimized circuits for primitive floating-point operations (addition, subtraction, multiplication, division, computing the square root, and comparison). We introduce circuits for integer operations in Appendix A. In this section, we denote integer-typed variables as Latin letters ( $a, b, \dots$ ), and floating-point values as Greek letters ( $\alpha, \beta, \dots$ ). To avoid verbosity, we assume familiarity with equality checks ( $=, C_{\text{isEq}}$ ), conditional selection ( $c ? t : f$ ), and boolean operations ( $\wedge, \vee, \neg, \oplus$ , etc.).

### 3.1 Initializing Floating-Point Numbers

Now we discuss how to initialize a floating-point number  $\alpha$  inside the circuit, whose original representation is  $\alpha = (\hat{s}, \hat{e}, \hat{m})$ , where  $\hat{s} \in \{0, 1\}$  is the sign bit,  $\hat{e}$  is an  $E$ -bit exponent, and  $\hat{m}$  is an  $M$ -bit mantissa (or significand). Note that although it is possible to represent  $\alpha$  in circuit as-is, we convert it to a compatible format  $\alpha = (s, e, m, a)$  to save as much constraints as possible, where  $s, e, m$  are circuit-efficient form of  $\hat{s}, \hat{e}, \hat{m}$ , and  $a \in \{0, 1\}$  is an additional bit indicating whether the number is abnormal.

**Shape Check.** On unchecked input  $\hat{s}, \hat{e}$ , and  $\hat{m}$  (which are usually secret witnesses), we first enforce that  $\hat{s}, \hat{e}$  and  $\hat{m}$  are well-formed

$C_{\text{FpRound}}(e, m, \Delta e, \text{aux} = 1)$

**Require:**  $m \in [0, 2^N - 1], \Delta e \in [0, K], 2^{N+K} < p$

- 1: Receive hints  $u', b_1, b_2, v' = H_{\text{Split}}(m \ll (K - \Delta e))$
- 2:  $C_{\text{RC}}(u', M); b_1(1 - b_1) = 0; b_2(1 - b_2) = 0; C_{\text{RC}}(v', N - M - 2 + K)$
- 3:  $m \ll K = (u' \parallel b_1 \parallel b_2 \parallel v') \ll \Delta e$
- 4:  $u := u' \parallel b_1; v := b_2 \parallel v'$
- 5:  $\text{half} := C_{\text{IsEq}}(v, 2^{N-M-2+K}) \wedge \text{aux}$
- 6:  $m' := (u + (\text{half} ? b_1 : b_2)) \ll \Delta e$
- 7:  $\text{overflow} := C_{\text{IsEq}}(m', 2^{M+1})$
- 8:  $e' := e + \text{overflow}$
- 9:  $m' := \text{overflow} ? 2^M : m'$
- 10: **return**  $e', m'$

**Figure 3: Circuit for rounding floating-point numbers**

in-circuit by checking  $\hat{s} \in \{0, 1\}, \hat{e} \in [0, 2^E - 1], \hat{m} \in [0, 2^M - 1]$ . After that, we initialize  $s := \hat{s}, e := \hat{e}, m := \hat{m}$ .

**Convert to Circuit Efficient Forms.** For a normal number  $\alpha = (-1)^s \cdot 2^{e-2^{E-1}+1} \cdot \overline{1.m}$ , we redefine  $e$  as the exponent's unbiased form, i.e.,  $e := e - 2^{E-1} + 1$ , and  $m$  as the mantissa with an explicit leading bit 1, i.e.,  $m := m + 2^M$ . In this way, we no longer need to handle the bias of  $e$  and the implicit leading bit of  $m$  in subsequent operations, thereby improving efficiency and clarity.

We convert subnormal numbers to normal numbers by normalizing their mantissas, allowing the exponents to 'underflow'. Specifically, for a subnormal number  $\alpha = (-1)^s \cdot 2^{-2^{E-1}+2} \cdot (0 \parallel m) \cdot 2^{-M}$ , we left shift the mantissa (with leading zero)  $0 \parallel m$ , and at the same time decrement the exponent  $-2^{E-1} + 2$  by 1, until the MSB (i.e.,  $M$ -th bit) of mantissa becomes 1. Denoting the shift by  $d \in [1, M]$ , we have  $\alpha = (-1)^s \cdot 2^{-2^{E-1}+2-d} \cdot ((0 \parallel m) \ll d) \cdot 2^{-M}$  and redefine  $e := -2^{E-1} + 2 - d, m := (0 \parallel m) \ll d = m \ll d$ . Now, the prover computes the hint  $d := H_{\text{Norm}}(v)$  and provides  $d$  to the circuit. For soundness, the circuit needs to check the predicate  $P_{\text{Norm}}(v, d)$  by calling  $C_{\text{RC}}((m \ll d) - (m_{\text{is}_0} ? 0 : 2^M), M)$ , which enforces  $m$  is zero or  $m \ll d \in [2^M, 2^{M+1} - 1]$ , implying that the MSB (i.e.,  $M$ -th bit) of a non-zero  $m \ll d$  is 1.

Normalizing unifies normal and subnormal numbers to save constraints in subsequent operations. Although subnormal numbers now take  $M + 1$  bits to represent, padding zeros do not contribute to precision, so they still have lower precision than normal numbers.

**Edge Cases.**  $\pm\infty$  is represented by  $e = 2^{E-1}, m = 2^M$ .  $\pm 0$  is represented by  $e = -2^{E-1} + 1 - M, m = 0$ . Although NaNs have different mantissas as per the specification, we always map them to fixed variables  $s = 0, e = 2^{E-1}, m = 0$  to simplify the handling of edge cases. We set 0 as NaN's mantissa due to the similar behaviors between NaNs and  $\pm 0$  in multiplication and division.

We compute the final exponent and mantissa inside the circuit using several conditional selections, and the entire in-circuit logic for initializing floating-point variables is described in Figure 2.

### 3.2 Rounding

The IEEE 754 standard requires the resulting mantissa of an operation to be rounded correctly and defines several rules specifying how and in which direction the rounding is done. Here, we discuss "rounding half to even" for binary encoded floating-point numbers.

This rule requires a decimal number to be rounded to the nearest integer, except when the fractional part is 0.5 (in base-10), the rounding should produce an even value, e.g.,  $0.5 \rightarrow 0, 1.5 \rightarrow 2$ .

Formally, consider an intermediate mantissa  $m \in [0, 2^N - 1]$  after some operation, and we are going to compute a rounded value  $m' \in [0, 2^l - 1]$ . First, we write  $m$  as  $m = u \parallel v$ , where  $u \in [0, 2^l - 1]$  and  $v \in [0, 2^{N-l} - 1]$ . We call  $v_{2^{N-l-1}}$  (the MSB of  $v$ ) the *guard bit*, and  $v_0 \vee \dots \vee v_{2^{N-l-2}}$  (the OR value of remaining bits of  $v$ ) the *sticky bit*. The round bit is not considered in our case, and rounding is done according to the guard bit and sticky bit. If guard bit is 0, i.e.,  $v \in [0, 2^{N-l-1})$ , the result is  $u$ . If guard bit is 1 and sticky bit is 0, i.e.,  $v = 2^{N-l-1}$ , the result is  $u + 1$  when  $u$  is odd and  $u$  when  $u$  is even. Otherwise,  $v \in (2^{N-l-1}, 2^{N-l})$ , and the result is  $u + 1$ .

Note that the upper bound of  $m'$  is  $2^l$  rather than  $2^l - 1$  due to the possible increment  $u_0$  or  $v_{N-l-1}$ . If  $m' = 2^l$ , i.e.,  $m'$  overflows, we set  $e' := e + 1, m' := 2^{l-1}$  to fix the overflow.

If we follow the standard exactly,  $l$  will be fixed to  $M+1$ . However, in our case,  $l = M+1$  only when the result is normal. For a subnormal number with an underflowed exponent  $e < -2^{E-1} + 2$ , we require  $l = M + 1 - \Delta e$ , where  $\Delta e = -2^{E-1} + 2 - e$  (here it is guaranteed that  $e \geq -2^{E-1} + 1 - M$ , implying  $l \geq 0$ ). The reason is that, for circuit efficiency, we pretend that subnormal numbers are normal when representing and operating on them. This works in most cases except for rounding, where subnormal numbers should actually be rounded with lower precision (i.e.,  $M + 1 - \Delta e$ ) than that of normal numbers (i.e.,  $M + 1$ ). Hence, we should only keep the first  $M + 1 - \Delta e$  bits of  $m$  for subnormal numbers. When the rounding is done, we left shift  $m'$  by  $\Delta e$  again to continue disguising them as normal.

Figure 3 illustrates the construction of the rounding gadget, where we require that  $\Delta e$  has a constant upper bound  $K$ , and that  $\Delta e = 0$  for normal numbers. First, we need to expand  $m$  into  $u \parallel v$  in-circuit. A naive approach is to ask the prover to provide  $u, v$  as hints, and the circuit checks  $u \in [0, 2^l - 1], v \in [0, 2^{N-l} - 1]$ . However, the upper bounds of  $u, v$  depend on the variable  $l$ . As discussed in Appendix A, a range check bounded by variables costs more constraints than a constant range check. To maximize circuit efficiency, the prover instead computes the hint  $H_{\text{Split}}$  by expanding  $m \ll (K - \Delta e)$  into  $u' \parallel b_1 \parallel b_2 \parallel v'$ , where  $u' \in [0, 2^{M-\Delta e} - 1], b_1, b_2 \in \{0, 1\}$  and  $v' \in [0, 2^{N-M-2+K} - 1]$ . Then  $u', b_1, b_2, v' := H_{\text{Split}}(m \ll (K - \Delta e))$  are fed to the circuit. Now,  $u := u' \parallel b_1, v := b_2 \parallel v'$ . To verify the predicate  $P_{\text{Split}}(m \ll (K - \Delta e), u', b_1, b_2, v')$ , the circuit checks the ranges of  $u'$  and  $v'$  by calling  $C_{\text{RC}}$ , enforces  $b_1$  and  $b_2$  are boolean, and asserts  $m \ll K = (u' \parallel b_1 \parallel b_2 \parallel v') \ll \Delta e$ . Moreover, as  $m$  is guaranteed to have length  $N$ , we can loosely bound  $u'$  and check  $u' \in [0, 2^M - 1]$  instead. This is safe, since if  $2^{M-\Delta e} \leq u' < 2^M$ , the length of  $u' \parallel b_1 \parallel b_2 \parallel v'$  will be longer than  $N + K - \Delta e$ , and  $m'$ 's length will be longer than  $N$ , which is a contradiction. Now, both range checks are bounded by constants.

After that, we compute  $\text{half} := C_{\text{IsEq}}(v, 2^{N-M-2+K}) \wedge \text{aux}$ , where, looking ahead,  $\text{aux}$  is the auxiliary information that helps determine the sticky bit in division and the computation of square root, and for a default  $\text{aux} = 1$ , the sticky bit solely depends on  $v$ . Then we have the rounded mantissa  $m' := (u + (\text{half} ? b_1 : b_2)) \ll \Delta e$ . Finally, we check  $\text{overflow} := C_{\text{IsEq}}(m', 2^{M+1})$ , and return the updated exponent and mantissa  $e' := e + \text{overflow}, m' := \text{overflow} ? 2^M : m'$ .

```

 $\alpha + \beta$ 
1:  $c, abs := C_{Abs}(e_\beta - e_\alpha, E + 1)$ 
2:  $e := c ? e_\beta : e_\alpha$ 
3:  $abs := C_{Min}(abs, M + 3)$ 
4:  $x := (c ? s_\beta m_\beta : s_\alpha m_\alpha) \ll L$ 
5:  $y := (c ? s_\alpha m_\alpha : s_\beta m_\beta) \ll (L - abs)$ 
6:  $z := x + y$ 
7:  $\neg s, m := C_{Abs}(z, 2M + 5)$ 
8:  $e := e + 1$ 
9:  $a := a_\alpha \vee a_\beta$ 
10:  $m\_is\_0 := C_{IsEq}(m, 0)$ 
11: Receive hint  $H_{Norm}(v) = d$ 
12:  $m := m \ll d; e := e - d$ 
13:  $C_{RC}(m - (m\_is\_0 ? 0 : 2^{2M+4}), 2M + 4)$ 
14:  $e', m' := C_{FpRound}(e, m, 0)$ 
15:  $a' := a \vee C_{GEZ}(e' - 2^{E-1}, E + 1)$ 
16:  $s' := C_{IsEq}(s_\alpha, s_\beta) ? s_\alpha : s$ 
17:  $e' := a' ? 2^{E-1} : (m\_is\_0 ? -2^{E-1} + 1 - M : e')$ 
18:  $m'_1 := (-a_\beta \vee C_{IsEq}(s_\alpha m_\alpha, s_\beta m_\beta)) ? m_\alpha : 0$ 
19:  $m'_2 := a_\beta ? m_\beta : (a' ? 2^M : m')$ 
20:  $m' := a_\alpha ? m'_1 : m'_2$ 
21: return  $s', e', m', a'$ 

```

Figure 4: Circuit for floating-point addition and subtraction

### 3.3 Addition And Subtraction

Adding two IEEE 754 floating-point numbers  $\alpha = (s_\alpha, e_\alpha, m_\alpha, a_\alpha)$  and  $\beta = (s_\beta, e_\beta, m_\beta, a_\beta)$  is done in the following 5 steps, and we depict the corresponding in-circuit logic in Figure 4. At a high level, addition requires 5 steps, described in the following: (i) aligning the exponent, (ii) adding the mantissa, (iii) normalizing and (iv) rounding the intermediate mantissa and (v) handling edge cases. Note, that subtraction is equivalent to addition by adding  $\alpha$  and  $-\beta$ .

**Align exponents (lines 1-3).** We first compare the exponents of  $\alpha$  and  $\beta$ . If  $e_\alpha \neq e_\beta$ , we need to align the exponents before performing the actual addition by shifting the mantissa of the number with smaller exponent to the *right* by  $abs := \text{abs}(e_\alpha - e_\beta)$  bits, such that the common exponent is  $e := \max(e_\alpha, e_\beta)$ . To avoid separately tracking the shifted bits (which will be used later in rounding), before performing the right shift, we first shift both mantissas to the *left* by  $L$  bits, where  $L$  is the upper bound of  $abs$ . That is, if  $e_\alpha > e_\beta$ , we compute  $x := m_\alpha \ll L, y := (m_\beta \ll L) \gg (e_\alpha - e_\beta)$ , and otherwise,  $x := m_\beta \ll L, y := (m_\alpha \ll L) \gg (e_\beta - e_\alpha)$ . The most significant  $M + 1$  bits of shifted mantissas contribute to the final result, and the remaining bits determine the rounding direction.

In circuit, we achieve this by computing  $c, abs := C_{Abs}(e_\beta - e_\alpha, E + 1)$  to obtain  $e := c ? e_\beta : e_\alpha$ . We observe that the final sum is only determined by  $x$  when  $y$  is completely shifted out, i.e., when  $abs \geq M + 3$ . Thus,  $abs > M + 3$  has the same effect as  $abs = M + 3$ . We improve the circuit efficiency by setting  $abs := C_{Min}(abs, M + 3)$ , so that it is no longer necessary to compute a large  $2^{abs}$ . Now,  $L = M + 3, x := (c ? m_\beta : m_\alpha) \ll L, y := (c ? m_\alpha : m_\beta) \ll (L - abs)$ .

**Add signed mantissas (lines 4-9).** Then we add the signed mantissas of adjusted  $\alpha$  and  $\beta$ , and obtain the resulting (signed) mantissa, i.e.,  $s \cdot m := s_\alpha \cdot x + s_\beta \cdot y$  if  $e_\alpha > e_\beta$ , and  $s \cdot m := s_\beta \cdot x + s_\alpha \cdot y$  otherwise. The sign  $s$  and unsigned mantissa  $m$  are extracted from the result, where  $m \leq x + y < 2(2^{M+1} \cdot 2^L) = 2^{2M+5}$ , i.e.,  $m$  has at most  $N = 2M + 5$  bits, among which the leading bit is caused by the possible carry. Thus, we also adjust the exponent as  $e := e + 1$ . For efficiency, we redefine the in-circuit variables

$x := (c ? s_\beta m_\beta : s_\alpha m_\alpha) \ll L, y := (c ? s_\alpha m_\alpha : s_\beta m_\beta) \ll (L - abs)$  to avoid extra conditional selection operations. Then we compute  $z := x + y$ , and compute  $s$  and  $m$  thanks to the  $C_{Abs}$  gadget:  $\neg s, m := C_{Abs}(z, N)$ . The result is abnormal if either input is abnormal, hence we have  $a := a_\alpha \vee a_\beta$ .

**Normalize intermediate mantissa (lines 10-13).** Normalization for  $m$  is the same as in Section 3.1 for normalizing subnormal numbers.  $m$  is shifted to the left by  $d$  bits, so that its MSB (i.e., the  $N - 1$ -th bit) becomes 1, unless  $m = 0$ , and  $e$  is decreased by  $d$ .

**Round intermediate mantissa (line 14).** The normalized mantissa  $m \ll d$  of length  $N$  is then rounded as in Section 3.2, with  $\Delta e = K = 0$ , obtaining  $e'$  and  $m'$ . Theoretically,  $\Delta e$  should be  $-2^{E-1} + 2 - e$ . However, we observe that for addition, a smaller  $\Delta e$  doesn't affect the result. In fact, it is safe to set  $\Delta e = 0$  to maximize circuit efficiency, and we explain the reasoning below.

Recall that the purpose of  $\Delta e$  is to limit the precision of subnormal numbers, but, as we will show later, the number of meaningful bits in  $m \ll d$  will never exceed the required precision, and the remaining bits are guaranteed to be zero. Consider a subnormal result with  $e \leq -2^{E-1} + 1$ , and assume, without loss of generality,  $e_\alpha < e_\beta$ . We denote  $\Delta e_\alpha = -2^{E-1} + 2 - e_\alpha, \Delta e_\beta = -2^{E-1} + 2 - e_\beta$ . Since  $e = \max(e_\alpha, e_\beta) + 1 - d = e_\beta + 1 - d$ , we have  $e_\alpha < e_\beta \leq -2^{E-1} + d$ . According to the rounding rule, we need to keep only  $M + 1 - (-2^{E-1} + 2 - e)$  bits in the mantissa, while the remaining  $N - (M + 1) + (-2^{E-1} + 2 - e) = L + d + \Delta e_\beta$  bits determine the rounding direction. Now we prove that the number of trailing zeros in  $m \ll d$  is at least  $L + d + \Delta e_\beta$  if  $e \leq -2^{E-1} + 1$ . Note, that  $x = s_\beta m_\beta \ll L, y = s_\alpha m_\alpha \ll (L - \min(e_\beta - e_\alpha, L)) = s_\alpha m_\alpha \ll \max(L - e_\beta + e_\alpha, 0)$ .

(i)  $\alpha$  subnormal,  $\beta$  subnormal – In this case,  $m_\alpha$  and  $m_\beta$  were left-shifted by  $\Delta e_\alpha$  and  $\Delta e_\beta$  bits when initialized. Also,  $e_\beta - e_\alpha \leq -2^{E-1} + 1 - (-2^{E-1} + 1 - M) = M < L$ , thus  $\max(L - e_\beta + e_\alpha, 0) = L - e_\beta + e_\alpha$ . Now,  $x$  has at least  $\Delta e_\beta + L$  trailing zeros, and  $y$  has at least  $\Delta e_\alpha + \max(L - e_\beta + e_\alpha, 0) = \Delta e_\alpha + L - e_\beta + e_\alpha = \Delta e_\beta + L$  trailing zeros. Hence,  $m \ll d$  has at least  $\Delta e_\beta + L + d$  trailing zeros.

(ii)  $\alpha$  subnormal,  $\beta$  normal – In this case,  $m_\alpha$  was left-shifted by  $\Delta e_\alpha$  bits when initialized. Now,  $x$  has at least  $L$  trailing zeros, and  $y$  has at least  $\Delta e_\alpha + \max(L - e_\beta + e_\alpha, 0) = \max(L + \Delta e_\beta, \Delta e_\alpha) < L$  trailing zeros. Consequently,  $m \ll d$  has at least  $\max(L + \Delta e_\beta, \Delta e_\alpha) + d \geq L + \Delta e_\beta + d$  trailing zeros.

(iii)  $\alpha$  normal,  $\beta$  normal – In this case,  $e_\beta - e_\alpha \leq -2^{E-1} + d - (-2^{E-1} + 2) = d - 2 < L$ , thus  $\max(L - e_\beta + e_\alpha, 0) = L - e_\beta + e_\alpha$ . Now,  $x$  has at least  $L$  trailing zeros, and  $y$  has at least  $\max(L - e_\beta + e_\alpha, 0) = L - e_\beta + e_\alpha < L$  trailing zeros. Consequently,  $m \ll d$  has at least  $L - e_\beta + e_\alpha + d$  trailing zeros, and  $L - e_\beta + e_\alpha + d \geq L + d + \Delta e_\beta$  because  $\Delta e_\beta + e_\beta - e_\alpha = \Delta e_\alpha \leq 0$ .

**Edge Cases (lines 15-21).** Finally, we need to handle the following:

- (i) If the mantissa  $m' = 0$  but  $e' \neq -2^{E-1} + 1 - M$  (which is possible, e.g., when computing  $1.0 - 1.0$ ), then canonicalize the exponent as  $e' := -2^{E-1} + 1 - M$ .
- (ii) If the exponent becomes too large, i.e.,  $e' \geq 2^{E-1}$ , then return  $\pm\infty$  (depending on the sign  $s$ ).
- (iii) If  $\alpha$  and  $\beta$  are  $\pm 0$ , return  $-0$  for  $-0 - 0$ , and otherwise,  $+0$ .
- (iv) If either  $\alpha$  or  $\beta$  is NaN, then return NaN.
- (v) If either  $\alpha$  or  $\beta$  is  $\pm\infty$ , then return NaN for  $\infty - \infty$  and  $-\infty + \infty$ , and otherwise,  $\pm\infty$  (depending on the sign  $s$ ).

```

 $\alpha \cdot \beta$ 
1:  $s := s_\alpha \oplus s_\beta; e := e_\alpha + e_\beta; m := m_\alpha \cdot m_\beta; a := a_\alpha \vee a_\beta$ 
2: Receive hint  $b = H_{\text{MSB}}(m)$ 
3:  $b(1-b) = 1; \text{CRC}(m - (b \ll (2M+1)), 2M+1)$ 
4:  $m := b ? m : m \ll 1; e := e + b$ 
5:  $\Delta e := C_{\text{Max}}(C_{\text{Min}}(-2^{E-1} + 2 - e, M+2, E+1), E+1)$ 
6:  $e', m' := C_{\text{FpRound}}(e, m, \Delta e)$ 
7:  $a' := a \vee C_{\text{GEZ}}(e' - 2^{E-1}, E+1)$ 
8:  $m'_{\text{is}_0} := C_{\text{IsEq}}(m', 0)$ 
9:  $e' := a' ? 2^{E-1} : (m'_{\text{is}_0} ? -2^{E-1} + 1 - M : e')$ 
10:  $m' := (a' \wedge \neg m'_{\text{is}_0}) ? 2^M : m'$ 
11: return  $s, e', m', a'$ 

```

Figure 5: Circuit for floating-point multiplication

```

 $\sqrt{\alpha}$ 
1:  $s := s_\alpha$ 
2: Receive hint  $b = H_{\text{LSB}}(e_\alpha)$ 
3:  $e := (e_\alpha - b)/2$ 
4:  $b(1-b) = 1; C_{\text{Abs}}(e, E-1)$ 
5: Receive hint  $n = H_{\text{Sqrt}}(m_\alpha \ll (M+4+b))$ 
6:  $r := (m_\alpha \ll (M+4+b)) - n^2$ 
7:  $\text{CRC}(r, M+4), \text{CRC}(2n-r, M+4)$ 
8:  $m := n$ 
9:  $m_{\text{is}_0} := C_{\text{IsEq}}(m_\alpha, 0)$ 
10:  $a := a_\alpha \vee (s_\alpha \wedge \neg m_{\text{is}_0})$ 
11:  $e', m' := C_{\text{FpRound}}(e, m, 0, C_{\text{IsEq}}(r, 0))$ 
12:  $e' := a ? 2^{E-1} : (m_{\text{is}_0} ? -2^{E-1} + 1 - M : e')$ 
13:  $m' := s ? 0 : m'$ 
14: return  $s, e', m', a$ 

```

Figure 6: Circuit for floating-point square root

(vi) Otherwise, return  $(s, e', m', 0)$  as the result.

To minimize the number of constraint, we unify some cases above based on the return value's exponent and mantissa in-circuit. First, the result is abnormal if either inputs is abnormal (iv, v), or the exponent is too large (ii). Hence,  $a' := a \vee C_{\text{GEZ}}(e' - 2^{E-1}, E+1)$ . Second, to support (iii), we set  $s' := C_{\text{IsEq}}(s_\alpha, s_\beta) ? s_\alpha : s$ . Third, the result's exponent is  $2^{E-1}$  if the result is abnormal (ii, iv, v), and is  $-2^{E-1} + 1 - M$  if the result is zero (i). Thus,  $e' := a' ? 2^{E-1} : (m_{\text{is}_0} ? -2^{E-1} + 1 - M : e')$ . Finally, for the result's mantissa  $m'$ , if both  $\alpha$  and  $\beta$  are abnormal,  $m' = 2^M$  for  $\infty + \infty$  and  $-\infty - \infty$  (v), and  $m' = 0$  otherwise (iv, v). If only one of  $\alpha$  and  $\beta$  is abnormal,  $m'$  equals the abnormal one's mantissa (iv, v). If both  $\alpha$  and  $\beta$  are normal, the result is  $2^M$  if the exponent becomes too large (ii). Lines 19-21 in Figure 4 summarize the logic above for handling  $m'$ .

### 3.4 Multiplication And Division

Multiplying two IEEE 754 floating-point numbers  $\alpha = (s_\alpha, e_\alpha, m_\alpha, a_\alpha)$  and  $\beta = (s_\beta, e_\beta, m_\beta, a_\beta)$  is done in the following 4 steps – (i) computing the product of  $\alpha$  and  $\beta$ , (ii) normalizing and (iii) rounding the intermediate mantissa and (iv) handling edge cases. We depict the corresponding in-circuit logic in Figure 5. The steps of division operation are highly similar to those of multiplication, and we defer their description to Appendix B due to the space limit.

**Compute product (line 1).** The product is negative only when one of  $\alpha$  and  $\beta$  is negative. Therefore, the sign of the product is  $s := s_\alpha \oplus s_\beta$ . The exponent and mantissa of the product are respectively  $e := e_\alpha + e_\beta$  and  $m := m_\alpha \cdot m_\beta$ . Since  $m_\alpha, m_\beta$  are either 0 or lie in  $[2^M, 2^{M+1} - 1]$ , a non-zero  $m$  should be bounded by  $m \in [2^{2M}, 2^{2M+2})$ . We further compute  $a := a_\alpha \vee a_\beta$ .

**Normalize intermediate mantissa (lines 2-4).** By leveraging the fact that  $m$  is either 0 or in  $[2^{2M}, 2^{2M+2})$ , the leading 1 of a non-zero  $m$  is either the  $2M$ -th bit or the  $2M+1$ -th bit. Hence, we can simplify the normalization process by checking if the  $2M+1$ -th bit of  $m$  is 1. If this is the case,  $m$  is already normal, and otherwise, we compute  $m := m \ll 1$ . Also,  $m_{2M+1} = 1$  indicates that the multiplication carries, and hence we increment  $e := e + 1$  if so. The improved normalization is done in-circuit as follows: the prover feeds  $b := H_{\text{MSB}}(m) = m_{2M+1}$ , the MSB of  $m$ , as a hint to circuit, and the circuit checks the predicate  $P_{\text{MSB}}(m, b)$  in 2 steps: (i) enforce  $b$  is a boolean, and (ii) assert  $m - (b \ll (2M+1)) \in [0, 2^{2M+1})$ . Then  $m, e$  are updated according to  $b$ , i.e.,  $m := b ? m : m \ll 1, e := e + b$ .

**Round intermediate mantissa (lines 5-6).** The normalized mantissa  $m$  of length  $N = 2M + 2$  is rounded by following the steps in Section 3.2, with  $\Delta e = \max(\min(-2^{E-1} + 2 - e, K), 0), K = M + 2$ , obtaining  $e'$  and  $m'$ .

**Edge Cases (lines 7-11).** Finally, we need to handle the following:

- (i) If the exponent becomes too large, i.e.,  $e' \geq 2^{E-1}$ , then return  $\pm\infty$  (depending on the sign  $s$ ).
- (ii) If the exponent becomes too small, i.e.,  $e' < -2^{E-1} + 1 - M$ , or equivalently, the rounded mantissa becomes 0, then return  $\pm 0$  (depending on the sign  $s$ ).
- (iii) If either  $\alpha$  or  $\beta$  is NaN, then return NaN.
- (iv) If either  $\alpha$  or  $\beta$  is  $\pm\infty$ , then return NaN for  $\pm 0 \cdot \pm\infty$  and  $\pm\infty \cdot \pm 0$ , and otherwise,  $\pm\infty$  (depending on the sign  $s$ ).
- (v) Otherwise, return  $(s, e', m', 0)$  as the result.

To minimize the number of constraint, we unify some cases above based on the return value's exponent and mantissa in-circuit. First, the result is abnormal if either input is abnormal (iii, iv), or the exponent is too large (i). Hence,  $a' := a \vee C_{\text{GEZ}}(e' - 2^{E-1}, E+1)$ . Second, the result's exponent is  $2^{E-1}$  if the result is abnormal (i, iii, iv), and is  $-2^{E-1} + 1 - M$  if the result is zero (ii). Thus,  $e' := a' ? 2^{E-1} : (m'_{\text{is}_0} ? -2^{E-1} + 1 - M : e')$ . Finally, the result's mantissa is only different from the rounded mantissa if the exponent is too large (i), or either inputs is  $\pm\infty$  and neither of them is  $\pm 0$  (iv). Both conditions are equivalent to the case where the result is abnormal but not NaN, so we have  $m' := (a' \wedge \neg m'_{\text{is}_0}) ? 2^M : m'$ .

### 3.5 Square Root Computation

The approximation of square roots is often based on the iterative Newton method [53]. To compute  $\beta = \sqrt{\alpha}$ , we first estimate an initial value  $\beta_0$ , and improve the accuracy in each round by computing  $\beta_{i+1} = \frac{1}{2}(\beta_i + \frac{\alpha}{\beta_i})$ . However, directly translating this approach to in-circuit operations introduces two challenges: (i) the number of iterations depends on how fast  $\sqrt{\alpha}$  converges, but handling loops conditioned on a variable in-circuit is hard, and (ii) each round of iteration requires one floating-point addition and one floating-point division, which are costly. To address (i), we need to run the loop for fixed number of rounds, taking the worst case for convergence into account, e.g., achieving the accuracy of FP64 needs 6 rounds of iteration in the worst case. We can resolve (ii) by computing the square root of the mantissa  $m_\alpha$  rather than the floating-point

value  $\alpha$ .  $\beta$ 's exponent can be obtained by halving  $e_\alpha$ . Since  $m_\alpha$  is an integer, addition and division in each round are cheap.

Nevertheless, this improved approach would easily cost hundreds of constraints due to the range checks caused by in-circuit integer division. To further reduce circuit size, we leverage the nondeterminism of the constraint system: the prover is asked to compute the square root of  $m_\alpha$  outside the circuit, and the circuit, given the square root as a hint, only needs to check its validity, thereby achieving the minimum cost. More specifically, we compute the square root of an IEEE 754 floating-point number  $\alpha = (s_\alpha, e_\alpha, m_\alpha, a_\alpha)$  inside the circuit in the following 4 steps, the process of which is also shown in Figure 6.

**Compute square root (lines 1-10).** First, we halve the exponent  $e_\alpha$ . When  $e_\alpha$  is even, we can simply compute  $e_\alpha/2$ , and otherwise, we need to calculate  $(e_\alpha - 1)/2$ . Combining both cases, the prover feeds  $b := H_{\text{LSB}}(e_\alpha)$ , the exponent's LSB, as a hint to circuit. The circuit checks the predicate  $P_{\text{LSB}}(e_\alpha, b)$  as follows: enforce  $b$  is boolean, compute  $e := (e_\alpha - b)/2$ , and assert  $e \in [-2^{E-1} + 1, 2^{E-1} - 1]$  by calling  $C_{\text{Abs}}(e, E - 1)$  (note that  $e$  might be negative). This guarantees that  $b$  is indeed the LSB of  $e_\alpha$ , as otherwise,  $e$  would be close to  $(p - 1)/2$  and its absolute value cannot fit into  $E - 1$  bits. Knowing the validity of  $b$ ,  $e$  is in fact in  $[-2^{E-2} - M/2, 2^{E-2}]$ . Next, we compute the mantissa's square root. To this end, the prover feeds the hint  $n := H_{\text{Sqrt}}(m_\alpha \ll (M + 4 + b)) = \sqrt{m_\alpha \ll (M + 4 + b)}$  to circuit, and the circuit checks the predicate  $P_{\text{Sqrt}}(m_\alpha \ll (M + 4 + b), n)$  by enforcing  $n^2 \leq (m_\alpha \ll (M + 4 + b)) < (n + 1)^2$  using two range checks. This guarantees that  $n$  is (the integer part of) the shifted mantissa's square root. We shift  $m_\alpha$  to the left before computing the square root for two reasons: (i) when  $e_\alpha$  is odd, we decrease it by 1, and thus the mantissa should be doubled when  $b = 1$ , or equivalently,  $m_\alpha \ll b$ , and (ii) the shift  $M + 4$  scales  $m_\alpha$  to achieve the desired precision. Otherwise, the result  $n$  would only have approx.  $M/2$  bits of precision. Successively, we obtain the intermediate mantissa  $m := n$ . Recall that the standard requires the intermediate result to have infinite precision, but  $m$  is not the exact square root. Thus, we apply the technique introduced in Appendix B: we further compute  $r := (m_\alpha \ll (M + 4 + b)) - n^2$ , which can help compute the sticky bit in rounding without storing the precise square root.

The result is abnormal if  $\alpha$  is abnormal or negative ( $-0$  is not included, as  $\sqrt{-0} = -0$ ). Hence, we set  $a := a_\alpha \vee (s_\alpha \wedge \neg C_{\text{IsEq}}(m_\alpha, 0))$ .

**Normalize intermediate mantissa.** Now, a non-zero  $m$ 's upper bound is  $\sqrt{(2^{M+1} - 1) \ll (M + 5)} < 2^{M+3}$ , and its lower bound is  $\sqrt{2^M \ll (M + 4)} = 2^{M+2}$ . Hence, the MSB (i.e.,  $M + 2$ -th bit) of  $m \in [2^{M+2}, 2^{M+3})$  is always 1 and normalization is unnecessary.

**Round intermediate mantissa (line 11).** The mantissa  $m$  of length  $N = M + 3$  is then rounded as in Section 3.2, with  $\Delta e = K = 0$ , obtaining  $e'$  and  $m'$ .  $\Delta e$  is fixed to 0 because the intermediate exponent  $e$  of a non-zero result is always greater than  $-2^{E-2} - M/2 > -2^{E-1} + 2$ , hence we don't need to handle the subnormal case. In addition, the equality between  $r$  and 0 is used to determine the sticky bit, thus we set the in-circuit parameter  $aux := C_{\text{IsEq}}(r, 0)$ .

**Edge Cases (lines 12-14).** Finally, we need to handle the following:

- (i) If  $\alpha$  is NaN, then return NaN.
- (ii) If  $\alpha$  is  $\pm\infty$ , then return  $\pm\infty$  (depending on the sign  $s$ )

$$\alpha < \beta$$

```

1: e_ge := CGEZ(e_alpha - e_beta, E + 1); m_ge := CGEZ(m_alpha - m_beta, M + 1)
2: s_lt := (C_IsEq(m_alpha, 0) & C_IsEq(m_beta, 0)) ? 0 : e_alpha
3: e_lt := s_alpha ? e_ge : ~e_ge
4: m_lt := C_IsEq(m_alpha, m_beta) ? 0 : (s_alpha ? m_ge : ~m_ge)
5: b := C_IsEq(s_alpha, s_beta) ? (C_IsEq(e_alpha, e_beta) ? m_lt : e_lt) : s_lt
6: b' := ((a_alpha & C_IsEq(m_alpha, 0)) v (a_beta & C_IsEq(m_beta, 0))) ? 0 : b
7: return b'

```

Figure 7: Circuit for floating-point comparison

(iii) If  $\alpha$  is negative, then return  $-0$  for  $\sqrt{-0}$ , and otherwise, NaN.

(iv) Otherwise, return  $(s, e', m', 0)$  as the result.

Thus, the final exponent is  $2^{E-1}$  when  $a = 1$ , is  $-2^{E-1} + 1 - M$  when  $m = 0$ , and is  $e'$  otherwise. Also, the rounded mantissa equals the expected final mantissa in all cases except (iii), where the final mantissa should be 0 if  $\alpha \leq 0$ . Hence we set  $m' := s_\alpha ? 0 : m'$ .

### 3.6 Comparison

Finally we discuss the comparison operation between two IEEE 754 floating-point numbers  $\alpha = (s_\alpha, e_\alpha, m_\alpha, a_\alpha)$  and  $\beta = (s_\beta, e_\beta, m_\beta, a_\beta)$  by introducing a circuit to determine whether  $\alpha < \beta$ . Other comparators like  $\leq, >, \geq$  can be constructed analogously.

First, we check if  $\alpha$  or  $\beta$  is NaN, in which case we return 0. Second, we compare the signs  $s_\alpha$  and  $s_\beta$ . If  $s_\alpha \neq s_\beta$ , then the result is 0 if  $\alpha = -0$  and  $\beta = +0$  ( $-0 = +0$ ), is 1 if  $s_\alpha$  is true but  $\alpha \neq -0$  (a negative value is always smaller than a positive one), and 0 otherwise. Now,  $s_\alpha = s_\beta$ . For the exponent, if  $e_\alpha \neq e_\beta$ , then the result equals  $e_\alpha < e_\beta$  for positive  $\alpha, \beta$  and  $e_\alpha > e_\beta$  for negative ones. Otherwise,  $\alpha$  and  $\beta$  have the same sign and exponent. We return  $m_\alpha < m_\beta$  for positive  $\alpha, \beta$  and  $m_\alpha > m_\beta$  for negative ones. We translate this logic to in-circuit operations built upon  $C_{\text{IsEq}}$  and  $C_{\text{GZ}}$  in Figure 7.

## 4 ZERO KNOWLEDGE LOCATION PRIVACY

In this section, we discuss the technical challenges when evaluating whether a location  $(\theta, \phi)$  is in a hexagonal tile  $\mathbf{h}$ . We provide a simplified description of the H3 protocol [54] that transforms spherical coordinates to hexagonal indices in Figure 8. In the following, we first describe how the baseline algorithm in the H3 hexagonal spatial indexing system transforms  $(\theta, \phi)$  into  $(i, j, k)$  coordinates, which uniquely identify a single hexagonal tile  $\mathbf{h}$  in the hexagonal grid. Successively, we highlight the difficulties when aiming to emulate the transformation in a SNARK circuit, and introduce optimizations that make the ZKLP paradigm practical.

**Transforming Spherical Coordinates to Coordinates in a Discrete Hexagonal Planar Grid Systems.** To utilize hexagonal hierarchical geospatial indexing, spherical coordinates (i.e.,  $(\theta, \phi)$ ) need to be converted to relative coordinates of the hexagon in the grid system of the geospatial index (i.e., the  $(i, j, k)$  coordinates). The H3 coordinate system deterministically maps  $(i, j, k)$  coordinates to H3 indices, and the  $(i, j, k)$  coordinates, in combination with the resolution  $res$ , are sufficient to determine a unique hexagon based on the latitude and longitude. In the following, we therefore solely describe the transformation of latitude and longitude to  $(i, j, k)$  coordinates in the hexagonal planar grid system of the H3 indexing system. The transformation relies on two logical steps:



$\Pi_{\text{Base}}(\theta, \phi, \text{res})$	
1: $(\theta_{\text{rad}}, \phi_{\text{rad}}) \leftarrow \text{ToRadians}(\theta, \phi)$	▷ Transform to Radians
2: $(x_u, y_u, z_u) \leftarrow \text{ToCartesian3D}(\theta_{\text{rad}}, \phi_{\text{rad}})$	▷ Transform to Cartesian
3: $d^2 = (x_F - x_u)^2 + (y_F - y_u)^2 + (z_F - z_u)^2$	▷ Distance to closest Face
4: $r \leftarrow \text{CalculateRadialDist}(d^2, \text{res})$	▷ Calculate the radial distance
5: $\sigma \leftarrow \text{CalculateAngle}(\theta_F, \phi_F, \theta, \phi)$	▷ Calculate angle to closest Face
6: $(x, y) \leftarrow \text{ToCartesian2D}(r, \sigma)$	▷ Calculate 2D Cartesian
7: $(I, J, K) = \text{TransformToIJK}(x, y)$	▷ Transform to "I,J,K"
8: <b>return</b> $(I, J, K)$	

**Figure 8: Baseline Protocol for computing  $(i, j, k)$  from  $(\theta, \phi)$ .**

*(1) Transforming spherical coordinates to Cartesian coordinates:*

The first step transforms a point from spherical coordinates to Cartesian coordinates in the 2D plane of an icosahedral face, specifically for the hexagonal grid system used in the H3 geospatial indexing system. Given geographic coordinates  $(\theta, \phi)$ , the distance from a given point on the sphere to the center of the closest face of the icosahedron is computed by evaluating the squared Euclidean distance  $d^2 = (x_2 - x_1)^2 + (y_2 - y_1)^2 + (z_2 - z_1)^2$ . To do so,  $(\theta, \phi)$  are converted to 3D Cartesian coordinates on a unit sphere:

$$\begin{aligned} z &= \sin(\theta) & x &= \cos(\phi) \cdot a \\ a &= \cos(\theta) & y &= \sin(\phi) \cdot a \end{aligned} \quad (1)$$

To determine the closest icosahedral face to  $(\theta, \phi)$ , the distance to each face is calculated individually. Given the squared Euclidean distance between two points on a sphere, the algorithm now aims to find the angular distance  $r$  between the two points when projected onto a unit sphere. The angular distance between two points on a sphere can be calculated using the spherical law of cosines and relates the sine of half the angular distance to the squared Euclidean distance between the points:  $\sin^2\left(\frac{r}{2}\right) = \frac{d^2}{4}$ , which can be transformed as  $\cos(r) = 1 - 2 \sin^2\left(\frac{r}{2}\right) = 1 - 2 \cdot \frac{d^2}{4} = 1 - \frac{d^2}{2}$ . This yields the angular distance as  $r = \arccos\left(1 - \frac{d^2}{2}\right)$ .

The algorithm performs a gnomonic projection of this angle by taking its tangent  $\tan(r)$ . The tangent function is used here to convert the angular distance  $r$  into a linear distance for the 2D plane. After the gnomonic scaling,  $r$  can be thought of as analogous to the radial distance in 2D polar coordinates. The radial distance is scaled according to the scaling factor from hexagonal grid unit length at resolution 0 to gnomonic unit length  $c_G$  given the desired H3 resolution  $\text{res}$ , such that  $r = \frac{r}{c_G} \cdot \sqrt{7}^{\text{res}}$ . Once the radial distance  $r$  is calculated, the counterclockwise angle  $\sigma$  between a reference direction on a given face of an icosahedron (for Uber H3 the  $i$ -axis of the Class II orientation [42]) and the direction from the center of that face to a point on the globe is determined. The radial distance  $r$  and the angle  $\theta$  together describe the polar coordinates of the  $(\theta, \phi)$  relative to the icosahedron face. The angle  $\sigma$  is calculated as the difference in azimuth (a type of angular measurement in a spherical coordinate system) between a reference axis on the icosahedron face and the azimuth from the center of that face to the given point. The azimuth values are normalized to be between 0 and  $2 \cdot \pi$ , such that  $\sigma = \text{norm}(\zeta_{F_i} - \text{norm}(\zeta(F_{\text{center}}, (\theta, \phi))))$ . The azimuth  $\zeta(p1, p2)$  from point  $p1$  to point  $p2$ , where  $\theta_1, \phi_1$  are the latitude and longitude of  $p1$ , and  $\theta_2, \phi_2$  are the latitude and longitude of  $p2$ , is calculated as  $\zeta(p1, p2) = \arctan\left(\frac{a}{b}\right)$ , with  $a = \cos(\theta_2) \sin(\Delta)$ ,  $b = \cos(\theta_1) \sin(\theta_2) - \sin(\theta_1) \cos(\theta_2) \cos(\Delta)$  and  $\Delta = \phi_2 - \phi_1$ .

In the H3 system, Class II and Class III orientations [48] alternate with each resolution. To adjust for the alternate orientation of hexagons at different resolutions, a constant rotation angle  $\arcsin\left(\sqrt{\frac{3}{28}}\right)$  is subtracted from  $\sigma$  if the chosen resolution is odd.

The remaining transformation transforms the coordinates  $(r, \sigma)$  to Cartesian coordinates  $(x, y)$  in the two-dimensional plane by computing  $x = r \cdot \cos(\sigma)$  and  $y = r \cdot \sin(\sigma)$ . The resulting coordinates  $(x, y)$  are the two-dimensional coordinates of the chosen hexagon relative to the face center of the closest icosahedron.

*(2) Transforming  $(x, y)$  coordinates to  $(i, j, k)$  coordinates:* The second step in obtaining coordinates in the discrete hexagonal planar grid system translates two-dimensional Cartesian coordinates  $(x, y)$  to three-dimensional coordinates  $(i, j, k)$ , uniquely identifying a hexagon at a given resolution. It is natural for the grid system to have three coordinate axis, spaced 120 degrees apart from each other, due to the structure of the underlying hexagons. The three-axis system allows for unique addressing without ambiguities [47].

The algorithm initially proceeds with quantization, setting  $k$  to 0 and operating on absolute values of  $(x, y)$ . If the value of  $(x, y)$  is not equivalent to the center of the hexagon, the continuous variables are rounded to the nearest hexagon center. To adjust for negative Cartesian coordinates, the Cartesian coordinates are folded across the axes to map them onto the hexagonal grid accordingly in  $(i, j, k)$  coordinates. Finally, the computed  $(i, j, k)$  coordinates are normalized to ensure that coordinates are as small as possible and non-negative. Normalizing the result is essential in ensuring that each hexagon in the grid has a unique address.

**Representing the Transformation as Constraints.** SNARKs work by encoding the computation in an arithmetic circuit over a finite field. In contrast, the transformation of geographic coordinates works over real numbers, represented in traditional programs as floating-point values. We address this issue by utilizing the circuits for primitive floating-point operations described in Section 3.

We still face the problem that our primitive operations in Section 3 do not aim to provide precise math functions ( $\sin, \cos, \tan, \dots$ ) as the IEEE standard does not specify the precision of math libraries. Even more so, a naive implementation would require approximation of math functions by the standard three-step recipe, as utilized in standard libraries – range reduction, polynomial approximation, and output compensation. Emulating polynomial approximations, by computing in-circuit Taylor Series, or applying the Remez algorithm [46], would lead to expensive increase in constraints due to high degree polynomials. Further, *precise* approximation is non-trivial, and standard techniques are inefficient without significant in-circuit optimization. Efficient algorithms for emulating accurate trigonometric functions are known for Two-Party-Computation [45]. However, we are not aware of any optimizations that lead to accurate and efficient in-circuit trigonometric approximations for SNARKs. We describe optimizations that fully eliminate trigonometric functions in our circuits as follows.

**Avoiding Trigonometric Operations.** Recall that transforming spherical coordinates to Cartesian coordinates demands *(i)* calculating the radial distance  $r$  of  $P_u$  to the closest icosahedral face (Step 4 in Figure 8), *(ii)* calculating the angle  $\sigma$  of  $P_u$  to the closest icosahedral face (Step 5 in Figure 8) and *(iii)* converting  $(r, \sigma)$  to

```

CZKLP( $\theta_{\text{rad}}, \phi_{\text{rad}}; \text{res}, I, J, K$ )
1: Receive  $H_{\text{ZKLP}}(i) = [\alpha_i, \beta_i, \gamma_i, \delta_i], i \in \{\theta_{\text{rad}}, \phi_{\text{rad}}\}$ 
2:  $\gamma_i^2 + \delta_i^2 = 1; \delta_i \cdot a_i = \gamma_i; 2\gamma_i \cdot d_i = \beta_i, i \in \{\theta_{\text{rad}}, \phi_{\text{rad}}\}$ 
3:  $r = \sqrt{1 - b_{\theta_{\text{rad}}}^2}; z = b_{\theta_{\text{rad}}}$ 
4:  $x = \sqrt{1 - b_{\phi_{\text{rad}}}^2} \cdot r; y = b_{\phi_{\text{rad}}} \cdot r$ 
5: for  $i \in \{0, \dots, 19\}$  do
6:    $d_i^2 = (x_{F_i} - x)^2 + (y_{F_i} - y)^2 + (z_{F_i} - z)^2$ 
7:    $d^2 = (d_i^2 < d^2) ? d_i^2 : d^2$ 
8:  $r \leftarrow C_{\text{rad}}(d^2, \text{res})$ 
9:  $\sin_i = \beta_i; \cos_i = \delta_i^2 - \gamma_i^2$  for  $i \in \{\theta_{\text{rad}}, \phi_{\text{rad}}\}$ 
10:  $(x, y) \leftarrow C_{\text{Hex2D}}(r, \text{res}, \sin_{\theta_{\text{rad}}}, \cos_{\theta_{\text{rad}}}, \sin_{\phi_{\text{rad}}}, \cos_{\phi_{\text{rad}}}, F_i)$ 
11:  $(i, j, k) \leftarrow C_{\text{ijk}}(x, y)$ 
12:  $C_{\text{isEq}}(i, I); C_{\text{isEq}}(j, J); C_{\text{isEq}}(k, K)$ 

```

Figure 9: Optimized Circuit for computing ZKLP.

```

Crad( $d^2, \text{res}$ )
1:  $r = \sqrt{\frac{-(d^2-4) \cdot d^2}{(2-d^2)}}; r = \frac{r}{c_G}$ 
2:  $\gamma := 1.0; c_\rho := \sqrt{7}$ 
3: for  $i \in \{1, \dots, R\}$  do
4:    $\gamma := (\text{res}[i]) ? \gamma \cdot c_\rho : \gamma$ 
5:    $c_\rho := c_\rho^2$ 
6: return  $(r \cdot \gamma)$ 

```

Figure 10: Optimized Sub-Circuit for computing the radial distance  $r$ .  $R$  represents the number of bits of res.

Cartesian coordinates  $(x, y)$  in the two-dimensional plane by computing  $x = r \cdot \cos(\sigma)$  and  $y = r \cdot \sin(\sigma)$  (Step 6 in Figure 8). We observe that we can avoid trigonometric operations altogether in the above steps by leveraging trigonometric identities.

To avoid evaluating trigonometric operations for computing the radial distance  $r$ , we substitute  $r = \arccos(1 - \frac{d^2}{2})$  into  $\tan(r)$ . By the Pythagorean identity, we express  $\tan(r) = \tan(\arccos(1 - \frac{d^2}{2}))$ .

$$r = \tan(r) = \sqrt{\frac{-(d^2 - 4) \cdot d^2}{(2 - d^2)}} \quad (2)$$

To minimize the number of constraints, we scale to the desired H3 resolution by applying the square and multiply algorithm for bit-wise exponentiation instead of naive exponentiation (cf. Figure 10).

Similarly, we simplify computing  $(x, y)$  with the angle  $\sigma$ . Recall that  $\sigma = \text{norm}(\zeta_{F_i} - \text{norm}(\zeta(F_{\text{center}}, (\theta, \phi))))$  where  $\zeta(p1, p2) = \arctan(\frac{p1}{p2})$ . By substituting the above values in the equations for calculating  $(x, y)$  and leveraging trigonometric identities, we obtain:

$$x = r \cdot \left( \cos(\theta_{F_i}) \frac{b}{\sqrt{a^2 + b^2}} + \sin(\theta_{F_i}) \frac{a}{\sqrt{a^2 + b^2}} \right)$$

$$y = r \cdot \left( \sin(\zeta_{F_i}) \frac{b}{\sqrt{a^2 + b^2}} - \cos(\zeta_{F_i}) \frac{a}{\sqrt{a^2 + b^2}} \right)$$

Note, that the trigonometric identities used in the simplification are mathematically sound regardless of normalization. As the center point of each icosahedron is fixed and known, the remaining sin and cos terms can be pre-computed. This representation is significantly less costly, as we already derived an optimized gadget for computing the square root of a floating-point variable in Section 3.5.

```

CHex2D( $r, \text{res}, \sin_{\theta_{\text{rad}}}, \cos_{\theta_{\text{rad}}}, \sin_{\phi_{\text{rad}}}, \cos_{\phi_{\text{rad}}}, F_i$ )
1:  $a := \sin_{\phi_{\text{rad}}} \cdot \cos_{\phi_{F_i, \text{rad}}}; b := \cos_{\phi_{\text{rad}}} \cdot \sin_{\phi_{F_i, \text{rad}}}$ 
2:  $c := \cos_{\theta_{F_i, \text{rad}}} \cdot \sin_{\theta_{\text{rad}}}; d := \sin_{\theta_{F_i, \text{rad}}} \cdot \cos_{\theta_{\text{rad}}}$ 
3:  $e := \cos_{\phi_{\text{rad}}} \cdot \cos_{\phi_{F_i, \text{rad}}}; f := \sin_{\phi_{\text{rad}}} \cdot \sin_{\phi_{F_i, \text{rad}}}$ 
4:  $x := c - d \cdot (e + g); y := \cos_{\theta_{\text{rad}}} \cdot (a - b); z := \sqrt{x^2 + y^2}$ 
5:  $\sin_{\zeta_{F_i}} := (\text{res}[0]) ? (\sin_{\zeta_{F_i}} - \arcsin(\sqrt{\frac{3}{28}})) : \sin_{\zeta_{F_i}}$ 
6:  $\cos_{\zeta_{F_i}} := (\text{res}[0]) ? (\cos_{\zeta_{F_i}} - \arcsin(\sqrt{\frac{3}{28}})) : \cos_{\zeta_{F_i}}$ 
7:  $\sin_\sigma := (\sin_{\zeta_{F_i}} \cdot \frac{x}{z}) - (\cos_{\zeta_{F_i}} \cdot \frac{y}{z})$ 
8:  $\cos_\sigma := (\cos_{\zeta_{F_i}} \cdot \frac{x}{z}) - (\sin_{\zeta_{F_i}} \cdot \frac{y}{z})$ 
9: return  $(r \cdot \sin_\sigma, r \cdot \cos_\sigma)$ 

```

Figure 11: Optimized Sub-Circuit for computing two-dimensional cartesian coordinates. Variables related to the face center  $F_i$  are constant floating-point numbers.

**Eliminating Trigonometric Operations with Hints.** It remains the complete elimination of trigonometric operations by avoiding the initial calculation of the Cartesian coordinates  $(x, y, z)$  from the user-supplied spherical coordinates  $(\theta, \phi)$  (cf. Equation 1). To do so, we observe that we can mindfully construct hints, such that the in-circuit computation reduces to (i) evaluating the hint predicate and (ii) calculating  $(x, y, z)$  without using trigonometric functions. As such, the hint  $H_{\text{ZKLP}}(\theta) = [\alpha_\theta, \beta_\theta, \gamma_\theta, \delta_\theta]$  is computed as  $\gamma_\theta = \sin(\frac{\theta}{2}), \delta_\theta = \cos(\frac{\theta}{2}), \beta_\theta = 2 \cdot \gamma_\theta \cdot \delta_\theta$  and  $\alpha_\theta = \tan(\frac{\theta}{2})$ .

Soundness holds as the in-circuit predicate  $P_{\text{ZKLP}}$  evaluates that (i)  $\gamma_\theta^2 + \delta_\theta^2$  equals 1, and thereby fulfills the fundamental trigonometric identity, (ii)  $\delta_\theta \cdot \alpha_\theta$  equals  $\gamma_\theta$ , which checks if the same angle is used, and (iii)  $2 \cdot \gamma_\theta \cdot \delta_\theta$  equals  $\beta_\theta$ , confirming that  $\beta_\theta$  is correctly related to  $\gamma_\theta$  and  $\delta_\theta$ . Afterwards, the  $x, y, z$  coordinates can simply be derived as  $z = \beta_\theta, r = \sqrt{1 - \beta_\theta^2}, x = \sqrt{1 - \beta_\theta^2} \cdot r$  and  $y = b_\phi \cdot r$ . As a result, trigonometric operations are eliminated from  $C_{\text{ZKLP}}$ . Note that  $\sin(i) = \beta_i$  and  $\cos(i) = \delta_i^2 - \gamma_i^2$  holds for  $i \in \{\theta, \phi\}$ .

**Transforming  $(x, y)$  to  $(i, j, k)$  coordinates.** The transformation is conducted by first transforming  $(x, y)$  to  $(i, j, k)$  coordinates and successively normalizing  $(i, j, k)$  coordinates to adjust for negative coordinates. We provide a detailed description of the sub-circuits for obtaining and normalizing  $(i, j, k)$  coordinates in Figure 18 and 19 in the appendix. They directly benefit from our floating-point implementation, due to many floating-point comparisons.

## 5 EMPIRICAL EVALUATION

Our empirical evaluation addresses three questions: (i) What is the performance and accuracy of our floating-point implementation?, (ii) How effective are our optimizations for the ZKLP paradigm?, and (iii) How tolerable is the cost of ZKLP in real-world use?

**Implementation.** We implement the floating-point primitive operations (cf. Section 3) as a reusable library in gnark [9]. We provide a full implementation of the optimized circuits for ZKLP (cf. Section 4) for FP32 and FP64 values. In addition, we implement the baseline protocol, without the optimizations as described in Section 4, over fixed-point arithmetic, where we convert floating-point values to fixed-point by multiplying by a scalar and rounding to

**Table 1: Number of R1CS constraints for in-circuit floating-point primitive operations, with  $|\mathcal{T}_{RC}| = 2^8$ ,  $|\mathcal{T}_{Pow2}| = 1 + E + M$** 

FP32 Operation	Init	Add/Sub	Mul	Div	Sqrt	Cmp	
# Native Constraints	13	42	31	38	23	26	
# Lookup Constraints	(i)	21	51	38	43	29	8
	(ii, iii)	291					
FP64 Operation	Init	Add/Sub	Mul	Div	Sqrt	Cmp	
# Native Constraints	13	42	31	38	23	26	
# Lookup Constraints	(i)	35	79	63	67	42	12
	(ii, iii)	323					

the nearest integer. Due to the agnostic nature of gnark, our implementation supports three SNARKs - Groth16, Plonk with KZG, and Plonk with FRI as a commitment scheme. We instantiate the lookup argument as LogUp [25], which is used in gnark for range checks. Our implementation and measurement data are open-sourced for reproducible results [15].

**Test Suite.** To ensure compliance with IEEE 754 [27], we generate a set of test values with the Berkeley TestFloat library [26], which generates test values to ensure that an implementation conforms to the IEEE Standard for Floating-Point Arithmetic. Specifically, 46464 test cases for each binary operation (e.g., Add), and 600 test cases for the unary operation Sqrt are created. Our implementation passes all these test cases, including inputs with abnormal values.

To evaluate the ZKLP circuit, we generate a series of geospatial points within hexagonal cells at various resolution levels, using Uber H3 implemented in C [54]. For a fixed resolution, we apply a logarithmic scale to generate nine points at varying distances from the cell center, with a sparser distribution of points closer to the center and denser as it approaches the boundary (cf. Figure 1).

**Experimental Setup.** When evaluating the runtime and memory consumption of a circuit, we execute all tests on an m6i.xlarge AWS instance with a 3.5 GHz Intel Xeon Ice Lake 8375C CPU and 16 GB of RAM. We report all values as the mean of 20 executions. The count of constraints is independent of the execution architecture.

## 5.1 Microbenchmarks and Comparison

We evaluate the cost of our circuits for floating-point operations (Section 3) and compare our implementation with existing works.

**Number of Constraints.** Table 1 presents the number of R1CS constraints for in-circuit floating-point primitive operations. Here, the size of  $\mathcal{T}_{RC}$  is fixed at  $2^8$ , and the size of  $\mathcal{T}_{Pow2}$  is 32 for FP32 and 64 for FP64. The constraints for each operation consist of two parts: native constraints (supported by the constraint system) and lookup constraints (for lookup tables). The inclusion of lookup constraints is necessary due to gnark’s implementation of LogUp [25]. Instead of running a separate protocol, gnark checks LogUp’s core equation  $\sum_{i=1}^{|f|} \frac{1}{X-f_i} = \sum_{i=j}^{|t|} \frac{m_j}{X-t_j}$  in the arithmetic circuit, resulting in a single SNARK proof for both the relation and the validity of lookup arguments. To eliminate lookup constraints, one can instantiate the lookup argument as standalone protocol and connect it to SNARK in a commit-and-prove fashion, at the cost of larger proofs.

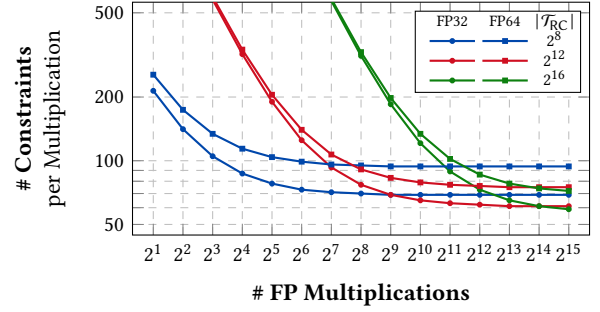


**Figure 12: Number of Constraints per Multiplication vs. Number of Multiplications, for Groth16.  $|\mathcal{T}_{RC}|$  is the size of the lookup table for the range check (cf. Section 3).**

Furthermore, the in-circuit verification of LogUp involves three steps: (i) compute the LHS  $\sum_{i=1}^{|f|} \frac{1}{X-f_i}$ , (ii) compute the RHS  $\sum_{i=j}^{|t|} \frac{m_j}{X-t_j}$ , where  $m_j$  is the number of occurrences for each entry  $t_j$ , and (iii) check the equality between the LHS and the RHS. As highlighted in the table, the costs of (ii) and (iii) are operation-agnostic; they only depend on the sizes of lookup tables  $\mathcal{T}_{RC}$  and  $\mathcal{T}_{Pow2}$ . Consequently, these costs remain unchanged as the number of queries increases. Therefore, they can be amortized across multiple operations.

Figure 12 shows the amortized cost of primitive operations, using multiplication as an example. With a larger  $\mathcal{T}_{RC}$ , the cost of step (ii) increases, while step (i) requires fewer constraints. This is particularly advantageous when proving the execution of many operations, as the one-time cost of steps (ii) and (iii) becomes negligible.

**Comparison With Other Works.** Naively converting FP32 operations compliant to IEEE 754 requires 2456 and 8854 boolean gates for addition and multiplication [56]. FP64 addition and multiplication requires 15637 and 44899 boolean gates respectively [3]. Garg *et al.* [20] provide the state-of-the-art succinct ZKP for floating-point operations, which requires 108 non-zero entries in the R1CS instance for FP32 addition and 25 for FP32 multiplication in a circuit over BN254. Due to the inconsistent metrics and our requirement of amortization, we are unable to present a fair comparison.

## 5.2 Privacy Preserving Location Proofs

Next, we evaluate the performance of an end-to-end implementation for the ZKLP circuits (Section 4) and an example application, privacy-preserving peer-to-peer proximity testing.

**Baseline Comparison & Optimizations.** We report the success rate of tests for fixed-point and floating-point implementations for emulating the transformation of  $(\theta, \phi)$  to  $(i, j, k)$  coordinates in a Zero-Knowledge Proof for resolutions 1 to 15 (Figure 13 in the appendix, due to lack of space). The fixed-point circuits emulate the baseline protocol without optimizations (cf. Figure 8), whereas the tests for floating-point circuits emulate the optimized  $C_{ZKLP}$  circuit (cf. Figure 9). In the fixed-point circuits, we approximate the trigonometric functions in-circuit, where  $\sin(x)$  is approximated by a Taylor Series and  $\arctan(x)$  is approximated by the Remez algorithm [46]. In our implementation for approximation of math functions, we apply the standard three-step recipe: *range reduction*, *polynomial approximation* and *output compensation* [12].

**Table 2: Evaluation of  $C_{ZKLP}$  for the floating-point implementation opposed to the baseline protocol  $\Pi_{Base}$  (cf. Figure 8), implemented with fixed-point arithmetic P6, over BN254. For Groth16, the SRS size is the size of the prover key.**

Circuit	Type	Proof System	# Constraints (x10 <sup>3</sup> )	Prover Time	Memory (MB)	SRS (MB)
	P6	Groth16	309.6	1.75 s	517.3	52.4
$C_{ZKLP}$	FP32	Groth16	21.9	0.27 s	272.2	4.8
	FP64	Groth16	27.6	0.38 s	271.7	6.5
	FP32	Plonk	62.5	2.20 s	268.9	2.1
	FP64	Plonk	89.0	4.41 s	269.4	4.2

We find that in the baseline protocol with a fixed-point circuit emulating 6 fractional bits, proving fails starting with resolution 11 (21.44 m to 8.14 m from the hexagon boundary). For the fixed-point implementation, all tests pass up to resolution 15 after adjusting the implementation to 8 fractional bits. Overall, we find that the constant scaling factor of the resolution ( $\sqrt{r^{res}}$ ) seems to have a significant impact on the accuracy of the computation.

Table 2 depicts the quantitative comparison of the fixed-point baseline and  $C_{ZKLP}$  implemented over our floating-point circuits. Our results show, that our optimizations applied for  $C_{ZKLP}$  are indeed very effective. When utilizing single precision floating-point, our circuit has 14.1× less constraints than the baseline, whereas when utilizing double precision floating-point, our circuit has 11.2× less constraints than the baseline. Note that the number of constraints in  $C_{ZKLP}$  remains constant, regardless of the chosen resolution. The proof generation time for both  $C_{ZKLP}$  over FP32 and FP64 is below 1 s for Groth16. With Plonk as a proof system, the time to generate a proof is higher, but remains in an acceptable range.

**P2P Proximity Testing.** We utilize the ZKLP paradigm to realize P2P proximity testing. Let  $\mathcal{H} = \{\mathbf{h}_1, \mathbf{h}_2, \dots, \mathbf{h}_n\}$  be a set of hexagons generated by the H3 system, where each hexagon  $\mathbf{h}$  is defined by its boundary vertices. Each vertex  $v_i$  of hexagon  $\mathbf{h}$  is given in geographical coordinates (latitude  $\theta_i$  and longitude  $\phi_i$ ). Given a user’s position  $P_u = (\theta_u, \phi_u)$ , the proximity to a hexagonal cell  $\mathbf{h}_v$  is evaluating the Haversine formula to calculate the great-circle distance between  $P_u$  and each vertex of  $\mathbf{h}_v$ . The Haversine distance  $\delta$  can be calculated as  $c = 2 \cdot \text{atan2}\left(\sqrt{a}, \sqrt{1-a}\right)$ , where  $a = \sin^2\left(\frac{\theta_2 - \theta_1}{2}\right) + \cos(\theta_1) \cdot \cos(\theta_2) \cdot \sin^2\left(\frac{\phi_2 - \phi_1}{2}\right)$ . Here,  $\theta_1, \phi_1$  and  $\theta_2, \phi_2$  are the latitude and longitude in radians of points  $P_u$  and a vertex of  $\mathbf{h}_v$ , respectively, and  $r$  is the radial length of the earth. The minimum distance  $\Delta_{\min}$  from point  $P_u$  to the boundary of hexagon  $\mathbf{h}_v$  is calculated as the smallest distance  $\Delta_{\min} = \min(\delta_0, \delta_1, \dots, \delta_i)$ . Calculating the proximity of  $P_u$  to the hexagonal boundary is done in plain and hence extremely efficient as compared to proving the ZKLP circuit. We implement proximity testing in Go, relying on the H3 library in C to determine the boundary points of the hexagon, and find that the computation requires  $\approx 2.58$  ms to execute, which is comparable to verifying a Groth16 proof ( $\approx 1.54$  ms). Hence, a verifier can evaluate its proximity to  $\approx 250$  peers per second.

## 6 RELATED WORKS

**Floating-Point Secure Computing.** To the best of our knowledge, there is no prior work supporting fully IEEE 754 compliant floating point computations for succinct proof systems. There are several prior works that investigate floating-point computations for secure computing [44]. Rathee *et al* provide IEEE 754 compliant functionalities for 2PC [45]. Closest to our work is the work of Garg *et al* [20]. However, their approach proves the upper bound of the relative error, and only supports addition and multiplication. Weng *et al* [56] use the IEEE 754 compliant single-precision boolean circuits from EMP-toolkit [55] for non-succinct ZKP computations.

**Location Privacy.** There is a long line of work on LPPM via ge-indistinguishability [1, 10, 49, 50, 51]. Narayanan *et al* [36] introduce location privacy via private proximity testing. Vsedenka *et al* [49] introduce interactive protocols for proximity testing over a spherical surface. In a similar setting, their protocols require  $> 1$  s and  $> 10$  kB communication. In contrast, our protocol is non-interactive and requires  $\approx 0.27$  s execution time (disregarding latency) and communicating a  $\approx 200$  Byte proof with Groth16. Babel *et al* [4] show how to evaluate whether a location is inbound a polygon. However, their approach assumes coordinates in  $(x, y)$  form in Euclidean plane. In comparison, our circuit for transforming  $(x, y)$  to a hexagonal index  $(C_{ijk})$  yields  $\approx 11.7\times$  less constraints. To the best of our knowledge, ZKLP provides the first paradigm for non-interactive, publicly verifiable and privacy preserving proofs of geolocation.

## 7 DISCUSSION & FUTURE WORK

To summarize, this paper introduces ZKLP (Section 4) via accurate floating-point SNARKs (Section 3), identifying a novel class of applications of general-purpose, succinct ZK proofs. The biggest challenge was ensuring accurate floating-point operations in finite fields without increasing constraints or compromising soundness.

In our experiments, we show that our implementation of floating-point arithmetic is efficient and accurate. We show that our instantiation of lookup tables amortizes the number of constraints per primitive operation. We show that the ZKLP paradigm is efficient, allowing users to generate an accurate proof in 0.27 s. We instantiate ZKLP with P2P proximity testing and show that a verifier can verify proximity to up 250 peers per second. Note, that the verification time and proof size is inherited by Groth16 [24, 13].

Yet, we acknowledge that our efforts fall short in ensuring *authentic* proofs of geographic location. Thus far, the input to our circuit is not bound to an actual location, i.e., obtained through GNSS, leading to a bootstrapping issue where a malicious prover could falsely prove any location. Common location-based services do not suffer from this problem due to a different trust and privacy model, e.g., GPS was designed for military use, before it was opened up for civilian applications. To solve this problem in our setting, we identify two potential solutions – (i) proving authenticated GNSS signals [23, 60] and (ii) utilizing TLS oracles [64, 33, 14]. To guide future work, we provide a detailed discussion in Appendix C.

Another interesting direction is applying our floating-point primitives and ZKLP in other domains. For instance, in machine learning, where parameters are often floating-point numbers [59], our methods could enable efficient, precise training [19] and inference proofs [30]. Further, we expect ZKLP to adapt naturally to other

settings. For example, ZKLP can be applied to develop privacy-preserving, location-based Smart Contract applications. Finally, we believe that authenticated ZKLP could be a useful building block in applications for Proof-of-Personhood to obtain verifiable location-based Sybil-resistance [8] and leave its exploration for future work.

## ACKNOWLEDGMENTS

The authors acknowledge the financial support by the Federal Ministry of Education and Research of Germany in the programme of “Souverän. Digital. Vernetzt.”. Joint project 6G-life, project identification number: 16KISK002.

## REFERENCES

- [1] Miguel E Andrés, Nicolás E Bordenabe, Konstantinos Chatzikokolakis, and Catuscia Palamidessi. 2013. Geo-indistinguishability: differential privacy for location-based systems. In *Proceedings of the 2013 ACM SIGSAC conference on Computer & communications security*, 901–914.
- [2] Sebastian Angel, Andrew J Blumberg, Eleftherios Ioannidis, and Jess Woods. 2022. Efficient representation of numerical optimization problems for {snarks}. In *31st USENIX Security Symposium (USENIX Security 22)*, 4273–4290.
- [3] David W. Archer, Shahla Atapoor, and Nigel P. Smart. 2021. The cost of IEEE arithmetic in secure computation. In *Progress in Cryptology – LATINCRYPT 2021*, 431–452.
- [4] Matthias Babel and Johannes Sedlmeir. 2023. Bringing data minimization to digital wallets at scale with general-purpose zero-knowledge proofs. *arXiv preprint arXiv:2301.00823*.
- [5] Eli Ben-Sasson, Iddo Bentov, Yinon Horesh, and Michael Riabzev. 2018. Scalable, transparent, and post-quantum secure computational integrity. *Cryptology ePrint Archive*.
- [6] Nir Bitansky, Ran Canetti, Alessandro Chiesa, and Eran Tromer. 2012. From extractable collision resistance to succinct non-interactive arguments of knowledge, and back again. In *Proceedings of the 3rd Innovations in Theoretical Computer Science Conference*, 326–349.
- [7] Jonathan Bootle, Andrea Cerulli, Jens Groth, Sune Jakobsen, and Mary Maller. 2018. Arya: nearly linear-time zero-knowledge proofs for correct program execution. In *International Conference on the Theory and Application of Cryptology and Information Security*. Springer, 595–626.
- [8] Maria Borge, Eleftherios Kokoris-Kogias, Philipp Jovanovic, Linus Gasser, Nicolas Gailly, and Bryan Ford. 2017. Proof-of-personhood: redemocratizing permissionless cryptocurrencies. In *2017 IEEE European Symposium on Security and Privacy Workshops (EuroS&PW)*. IEEE, 23–26.
- [9] [SW] Gautam Botrel, Thomas Piellard, Youssef El Housni, Ivo Kubjas, and Arya Tabaie, ConsenSys/gnark: v0.9.0 version v0.9.0, Feb. 2023. doi: 10.5281/zenodo.5819104, URL: <https://doi.org/10.5281/zenodo.5819104>.
- [10] Spyros Boukoros, Mathias Humbert, Stefan Katzenbeisser, and Carmela Troncoso. 2019. On (the lack of) location privacy in crowdsourcing applications. In *28th USENIX Security Symposium (USENIX Security 19)*, 1859–1876.
- [11] Matteo Campanelli, Antonio Faonio, Dario Fiore, Tianyu Li, and Helger Lipmaa. 2023. *Lookup Arguments: Improvements, Extensions and Applications to Zero-Knowledge Decision Trees*. Ph.D. Dissertation. IACR Cryptology ePrint Archive.
- [12] William James Cody. 1980. *Software Manual for the Elementary Functions (Prentice-Hall series in computational mathematics)*. Prentice-Hall, Inc.
- [13] Jens Ernstberger, Stefanos Chaliasos, George Kadianakis, Sebastian Steinhorst, Philipp Jovanovic, Arthur Gervais, Benjamin Livshits, and Michele Orrù. 2023. Zk-bench: a toolset for comparative evaluation and performance benchmarking of snarks. *Cryptology ePrint Archive*.
- [14] Jens Ernstberger, Jan Lauinger, Yinnan Wu, Arthur Gervais, and Sebastian Steinhorst. 2024. Origo: proving provenance of sensitive data with constant communication. *Cryptology ePrint Archive*.
- [15] 2024. Floating point and zkfp open-source implementation. <https://github.com/tumberger/zk-Location/>. (2024).
- [16] Ariel Gabizon and Zachary J Williamson. 2020. Plookup: a simplified polynomial protocol for lookup tables. *Cryptology ePrint Archive*.
- [17] Ariel Gabizon, Zachary J Williamson, and Oana Ciobotaru. 2019. Plonk: permutations over lagrange-bases for oecumenical noninteractive arguments of knowledge. *Cryptology ePrint Archive*.
- [18] Aleix Galan, Ignacio Fernandez-Hernandez, Luca Cucchi, and Gonzalo Seco-Granados. 2022. Osmnalib: an open python library for galileo osnma. In *2022 10th Workshop on Satellite Navigation Technology (NAVITEC)*. IEEE, 1–12.
- [19] Sanjam Garg, Aarushi Goel, Suresh Jha, Saeed Mahloujifar, Mohammad Mahmood, Guru-Vamsi Policharla, and Mingyuan Wang. 2023. Experimenting with zero-knowledge proofs of training. In *Proceedings of the 2023 ACM SIGSAC Conference on Computer and Communications Security*, 1880–1894.
- [20] Sanjam Garg, Abhishek Jain, Zhengzhong Jin, and Yinuo Zhang. 2022. Succinct zero knowledge for floating point computations. In *Proceedings of the 2022 ACM SIGSAC Conference on Computer and Communications Security*, 1203–1216.
- [21] Rosario Gennaro, Craig Gentry, Bryan Parno, and Mariana Raykova. 2013. Quadratic span programs and succinct nzkz without pcps. In *Advances in Cryptology—EUROCRYPT 2013: 32nd Annual International Conference on the Theory and Applications of Cryptographic Techniques, Athens, Greece, May 26–30, 2013. Proceedings 32*. Springer, 626–645.
- [22] Google. 2024. Google geolocation api. <https://developers.google.com/maps/documentation/geolocation/overview>. (2024).
- [23] Martin Götzelmann, Evelyn Köller, Ignacio Viciano-Semper, Dirk Oskam, Elias Gkougkas, and Javier Simon. 2023. Galileo open service navigation message authentication: preparation phase and drivers for future service provision. *NAVIGATION: Journal of the Institute of Navigation*, 70, 3.
- [24] Jens Groth. 2016. On the size of pairing-based non-interactive arguments. In *Annual international conference on the theory and applications of cryptographic techniques*. Springer, 305–326.
- [25] Ulrich Haböck. 2022. Multivariate lookups based on logarithmic derivatives. *Cryptology ePrint Archive*.
- [26] John Hauser. 2018. Berkeley testfloat release 3e. <https://github.com/ucb-bar/berkeley-testfloat-3>. (2018).
- [27] 2019. IEEE standard for floating-point arithmetic. *IEEE Std 754-2019 (Revision of IEEE 754-2008)*, 1–84. doi: 10.1109/IEEESTD.2019.8766229.
- [28] Kai Jansen, Matthias Schäfer, Daniel Moser, Vincent Lenders, Christina Pöpper, and Jens Schmitt. 2018. Crowd-gps-sec: leveraging crowdsourcing to detect and localize gps spoofing attacks. In *2018 IEEE Symposium on Security and Privacy (SP)*. IEEE, 1018–1031.
- [29] Hongbo Jiang, Jie Li, Ping Zhao, Fanzi Zeng, Zhu Xiao, and Arun Iyengar. 2021. Location privacy-preserving mechanisms in location-based services: a comprehensive survey. *ACM Computing Surveys (CSUR)*, 54, 1, 1–36.
- [30] Daniel Kang, Tatsunori Hashimoto, Ion Stoica, and Yi Sun. 2022. Scaling up trustless dnn inference with zero-knowledge proofs. *arXiv preprint arXiv:2210.08674*.
- [31] Daniel Kang, Tatsunori Hashimoto, Ion Stoica, and Yi Sun. 2022. Zk-ing: attested images via zero-knowledge proofs to fight disinformation. *arXiv preprint arXiv:2211.04775*.
- [32] Ali Khoshgozaran and Cyrus Shahabi. 2007. Blind evaluation of nearest neighbor queries using space transformation to preserve location privacy. In *International symposium on spatial and temporal databases*. Springer, 239–257.
- [33] Jan Lauinger, Jens Ernstberger, Andreas Finkenzeller, and Sebastian Steinhorst. 2023. Janus: fast privacy-preserving data provenance for tls 1.3. *Cryptology ePrint Archive*.
- [34] Byoungyoung Lee, Jinoh Oh, Hwanjo Yu, and Jong Kim. 2011. Protecting location privacy using location semantics. In *Proceedings of the 17th ACM SIGKDD international conference on Knowledge discovery and data mining*, 1289–1297.
- [35] Todd Litman. 2007. Distance-based vehicle insurance feasibility, costs and benefits. *Victoria*, 11.
- [36] Arvind Narayanan, Narendran Thiagarajan, Mugdha Lakhani, Michael Hamburg, Dan Boneh, et al. 2011. Location privacy via private proximity testing. In *NDSS*. Vol. 11.
- [37] Assa Naveh and Eran Tromer. 2016. Photoproof: cryptographic image authentication for any set of permissible transformations. In *2016 IEEE Symposium on Security and Privacy (SP)*. IEEE, 255–271.
- [38] Alexandra-Mihaela Olteanu, Kevin Huguenin, Reza Shokri, Mathias Humbert, and Jean-Pierre Hubaux. 2016. Quantifying interdependent privacy risks with location data. *IEEE Transactions on Mobile Computing*, 16, 3, 829–842.
- [39] OpenStreetMaps. 2024. Openstreetmap. <https://www.openstreetmap.org/>. (2024).
- [40] OpenStreetMaps. 2023. Openstreetmap statistics. [https://planet.openstreetmap.org/statistics/data\\_stats.html](https://planet.openstreetmap.org/statistics/data_stats.html). (2023).
- [41] Raluca Ada Popa, Hari Balakrishnan, and Andrew J Blumberg. 2009. Vpriv: protecting privacy in location-based vehicular services.
- [42] Edward S Popko and Christopher J Kitrick. 2021. Divided spheres. In *Divided Spheres*. AK Peters/CRC Press, 1–12.
- [43] Jim Posen and Assimakis A Kattis. 2022. Caulk+: table-independent lookup arguments. *Cryptology ePrint Archive*.
- [44] Pille Pullonen and Sander Siim. 2015. Combining secret sharing and garbled circuits for efficient private IEEE 754 floating-point computations. In *Financial Cryptography and Data Security: FC 2015 International Workshops, BITCOIN, WAHC, and Wearable, San Juan, Puerto Rico, January 30, 2015, Revised Selected Papers 19*. Springer, 172–183.
- [45] Deevashwer Rathee, Anwesh Bhattacharya, Rahul Sharma, Divya Gupta, Nishanth Chandran, and Aseem Rastogi. 2022. Secfloat: accurate floating-point meets secure 2-party computation. In *2022 IEEE Symposium on Security and Privacy (SP)*. IEEE, 576–595.
- [46] Eugene Y Remez. 1934. Sur la détermination des polynômes d’approximation de degré donnée. *Comm. Soc. Math. Kharkov*, 10, 196, 41–63.

- [47] Kevin Sahr. 2019. Central place indexing: hierarchical linear indexing systems for mixed-aperture hexagonal discrete global grid systems. *Cartographica: The International Journal for Geographic Information and Geovisualization*, 54, 1, 16–29.
- [48] Kevin Sahr, Denis White, and A Jon Kimerling. 2003. Geodesic discrete global grid systems. *Cartography and Geographic Information Science*, 30, 2, 121–134.
- [49] Jaroslav Šeděnka and Paolo Gasti. 2014. Privacy-preserving distance computation and proximity testing on earth, done right. In *Proceedings of the 9th ACM symposium on Information, computer and communications security*, 99–110.
- [50] Reza Shokri, George Theodorakopoulos, Jean-Yves Le Boudec, and Jean-Pierre Hubaux. 2011. Quantifying location privacy. In *2011 IEEE symposium on security and privacy*. IEEE, 247–262.
- [51] Reza Shokri, George Theodorakopoulos, Carmela Troncoso, Jean-Pierre Hubaux, and Jean-Yves Le Boudec. 2012. Protecting location privacy: optimal strategy against localization attacks. In *Proceedings of the 2012 ACM conference on Computer and communications security*, 617–627.
- [52] Tomer Solberg. 2023. A brief history of lookup arguments. <https://github.com/ingonyama-zk/papers/blob/main/lookups.pdf>. (2023).
- [53] Endre Süli and David F Mayers. 2003. *An introduction to numerical analysis*. Cambridge university press.
- [54] Uber. 2023. Uber hexagonal hierarchical spatial index. <https://www.uber.com/en-DE/blog/h3/>. (2023).
- [55] Xiao Wang, Alex J. Malozemoff, and Jonathan Katz. 2016. EMP-toolkit: Efficient MultiParty computation toolkit. <https://github.com/emp-toolkit>. (2016).
- [56] Chenkai Weng, Kang Yang, Xiang Xie, Jonathan Katz, and Xiao Wang. 2021. Mystique: efficient conversions for {zero-knowledge} proofs with applications to machine learning. In *30th USENIX Security Symposium (USENIX Security 21)*, 501–518.
- [57] Xiang Xie, Kang Yang, Xiao Wang, and Yu Yu. 2023. Lightweight authentication of web data via garble-then-prove. *Cryptology ePrint Archive*.
- [58] Alex Luoyuan Xiong, Binyi Chen, Zhenfei Zhang, Benedikt Bünz, Ben Fisch, Fernando Krell, and Philippe Camacho. 2023. {Verizexe}: decentralized private computation with universal setup. In *32nd USENIX Security Symposium (USENIX Security 23)*, 4445–4462.
- [59] Thomas Yeh, Max Sterner, Zerlina Lai, Brandon Chuang, and Alexander Ihler. 2022. Be like water: adaptive floating point for machine learning. In *International Conference on Machine Learning*. PMLR, 25490–25500.
- [60] Muzi Yuan, Xiaomei Tang, and Gang Ou. 2023. Authenticating gnss civilian signals: a survey. *Satellite Navigation*, 4, 1, 1–18.
- [61] Arantxa Zapico, Vitalik Buterin, Dmitry Khovratovich, Mary Maller, Anca Nitulescu, and Mark Simkin. 2022. Caulk: lookup arguments in sublinear time. In *Proceedings of the 2022 ACM SIGSAC Conference on Computer and Communications Security*, 3121–3134.
- [62] Arantxa Zapico, Ariel Gabizon, Dmitry Khovratovich, Mary Maller, and Carla Rafols. 2022. Baloo: nearly optimal lookup arguments. *Cryptology ePrint Archive*.
- [63] Kexiong Curtis Zeng, Shinan Liu, Yuanchao Shu, Dong Wang, Haoyu Li, Yanzhi Dou, Gang Wang, and Yaling Yang. 2018. All your {gps} are belong to us: towards stealthy manipulation of road navigation systems. In *27th USENIX security symposium (USENIX security 18)*, 1527–1544.
- [64] Fan Zhang, Deepak Maram, Harjasleen Malvai, Steven Goldfeder, and Ari Juels. 2020. Deco: liberating web data using decentralized oracles for tls. In *Proceedings of the 2020 ACM SIGSAC Conference on Computer and Communications Security*, 1919–1938.

## A CIRCUITS FOR INTEGER OPERATIONS

Only operations in the prime field  $\mathbb{F}_p$  are natively supported by arithmetic circuits, and thus supporting in-circuit integer operations in an efficient and sound way is non-trivial. We introduce circuits for integer-typed values  $v$  for checking that  $v \in [0, 2^L - 1]$ , computing sign, absolute, maximum and minimum value of  $v$ , and shifting left  $\ll$  and right  $\gg$  in the following.

**Range Check.** Bit decomposition is a standard technique for ensuring that a variable  $v \in \mathbb{F}_p$  is an  $L$ -bit string, i.e.,  $v \in [0, 2^L - 1]$ . The prover first provides the decomposition as a hint to the circuit by computing  $H_{\text{Dec}}(v) = \{v_0, \dots, v_{L-1}\}$ . The predicate  $P_{\text{Dec}}$  for verifying the bit decomposition of  $v$  into  $\{v_0, \dots, v_{L-1}\}$  asserts that all variables are boolean by checking  $v_i(1 - v_i) = 0$  for all  $i \in [0, L - 1]$ , and that  $v$  is indeed composed of  $\{v_0, \dots, v_{L-1}\}$  by

asserting  $\sum_{i=0}^{L-1} 2^i v_i = v$ , such that

$$P_{\text{Dec}}(v, \{v_0, \dots, v_{L-1}\}) = \begin{cases} 1 & \text{if } v = \sum_{i=0}^{L-1} 2^i v_i \wedge \\ & v_i(1 - v_i) = 0 \forall i \in [0, L - 1], \\ 0 & \text{otherwise.} \end{cases}$$

$L$  should satisfy  $2^L < p$ , so that the summation of  $2^i v_i$  does not overflow the field order. For  $a$  and  $b$  known to be  $L$ -bit strings, this method can be extended to ensure  $v \in [a, b]$  by decomposing  $v - a$  and  $b - v$  separately into  $L$  bits.

However, the bit decomposition approach requires  $O(L)$  constraints, which is not optimal. In fact, we can improve the circuit efficiency by leveraging lookup argument. We build a lookup table  $\mathcal{T}_{\text{RC}}$  with entries  $\{0, \dots, 2^T - 1\}$ . On inputs  $v, L$ , the circuit  $C_{\text{RC}}$  now requires the prover to compute the hint  $H_{\text{Dec}'}(v)$  by decomposing  $v$  into  $T$ -bit strings  $v'_0, \dots, v'_{L/T-1}$ . Then the circuit checks the predicate  $P_{\text{Dec}'}(v, \{v'_0, \dots, v'_{L/T-1}\})$  by merging the set  $\{v'_0, \dots, v'_{L/T-1}\}$  into the vector of queries  $\mathbf{t}_{\text{RC}}$  and enforcing  $v = \sum_{i=0}^{L/T-1} 2^{iT} v'_i$ .

The  $C_{\text{RC}}$  circuits based on both approaches for checking  $v \in [0, 2^L - 1]$  are described in Figure 14.

**Sign and Absolute Value.** Obtaining the sign and the  $L$ -bit absolute value of a variable  $v \in \mathbb{F}_p$  presents a more complex challenge. Intuitively, a number is positive if it is greater than 0, and is negative otherwise. However, as the field  $\mathbb{F}_p$  is not *ordered*, we cannot *compare* between its elements. To address this, we manually define elements in the set  $\{1, 2, \dots, (p - 1)/2\}$  as positive, and those in the set  $\{(p + 1)/2, \dots, p - 2, p - 1\}$  as negative. Now, as long as  $2^L < (p - 1)/2$ , we can extract the sign and the absolute value of  $v$  as depicted in  $C_{\text{Abs}}$  in Figure 15. The prover determines if  $v$  is positive by checking which set it belongs to, and provides  $H_{\text{GEZ}} = s$  as a hint to the circuit. The gadget enforces that  $s$  is boolean, and computes  $v$ 's absolute value  $abs$ , which is  $v$  if  $s$  is 1, and is  $-v$  otherwise. Finally, the gadget enforces that  $abs$  has at most  $L$  bits and returns  $abs$  and  $s$ . Soundness holds because if an adversary feeds the incorrect  $s$  to the circuit, then  $abs$ 's value belongs to the negative set and is hence greater than  $(p - 1)/2$ , but  $C_{\text{RC}}$  is later used to guarantee that  $abs < 2^L < (p - 1)/2$ .

**Maximum and Minimum.** Given  $C_{\text{Abs}}$ , it is straightforward to build circuits for computing the maximum and minimum values between  $x$  and  $y$  whose difference has  $L$  bits, which, as listed in Figure 15, is done by calling  $C_{\text{Abs}}$  on  $x - y$  and select  $x$  or  $y$  based on the sign of the difference.  $C_{\text{Max}}$  and  $C_{\text{Min}}$  forward  $x - y$  and  $L$  to  $C_{\text{Abs}}$ , where  $C_{\text{Abs}}$  returns the sign bit  $s$  only.

**Shifting.** Figure 16 summarizes the circuits for shifting left  $\ll$  and right  $\gg$ . The core component of shift operations is computing powers of 2 in-circuit. We are interested in  $2^d$  with a variable exponent  $d$  (for a constant exponent  $D$ ,  $2^D$  is also a constant and does not involve any constraints), which is assumed to be a  $K$ -bit integer and  $2^K < p$ . One approach to compute  $2^d$  is to leverage the square-and-multiply algorithm. That is, we decompose  $d$  into  $K$  bits  $d_0, \dots, d_{K-1}$  and select the term  $2^{2^i}$  or 1 based on the value of  $d_i$ . The product of these terms is the result  $2^d$ . Although this method is already efficient, it still requires  $O(K)$  constraints. For example, in RICS, we need  $K + 1$  constraints for bit decomposition and  $K - 1$  constraints for multiplying  $K$  terms, resulting in  $2K$  constraints



Figure 13: Testing ZKLP for resolutions 1 to 15 for fixed-point (P6, P12), single precision (FP32) and double precision (FP64) floating-point values. For a given resolution, test cases logarithmically approach the boundary of a given hexagon. If a cell is green, proof generation succeeds. If a cell is red, proof generation fails. All tests are executed for Groth16 over curve BN254.

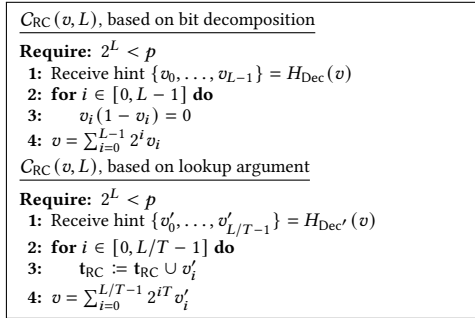


Figure 14: Circuit for checking  $v \in [0, 2^L - 1]$ .

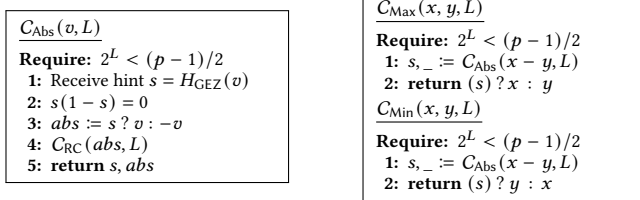


Figure 15: Circuits for computing sign and absolute value ( $C_{Abs}$ ) as well as maximum ( $C_{Max}$ ) & minimum values ( $C_{Min}$ ).

in total. This is not ideal, especially for our case where the shift operation is frequently used. In order to minimize circuit size, we introduce  $\mathcal{T}_{Pow2}$ , a lookup table for  $2^d$ .

$\mathcal{T}_{Pow2}$  is first populated with entries, where the  $i$ -th entry is  $f_i = (i, 2^i)$ . To compute a query to the lookup table for the variable

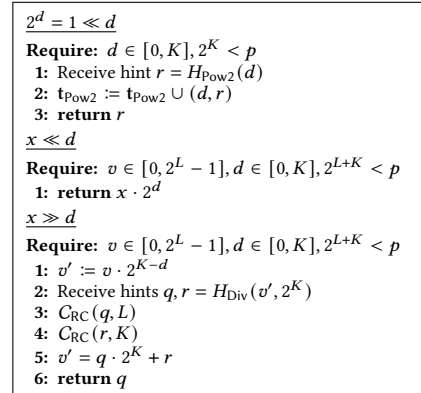


Figure 16: Circuits for shift operations

exponent  $d$ , we compute  $2^d$  with a hint and append  $(d, 2^d)$  to the vector of queries  $t_{Pow2}$ . Successively, we check that  $t_{Pow2} \in \mathcal{T}_{Pow2}$ . The returned result is  $2^d$ , where soundness holds due to the lookup argument.

The construction of left shift gadget  $v \ll d$  is safe and straightforward, assuming that  $v \in [0, 2^L - 1]$  and  $d \in [0, K]$ , such that  $2^{L+K} < p$ ; we only need to compute  $2^d$  and then return  $v \cdot 2^d$ .

Constructing an efficient right shift gadget  $v \gg d$  needs non-trivial techniques. Here, we also assume that  $v \in [0, 2^L - 1]$ ,  $d \in [0, K]$ , and  $2^{L+K} < p$ . Naively, we could treat the right shift operation as integer division, i.e.,  $v \gg d = v/2^d$ . The prover computes the quotient  $q$  and the remainder  $r$  such that  $v = q \cdot 2^d + r$ , and feeds

$\alpha \div \beta$	
1:	$s := s_\alpha \oplus s_\beta$
2:	$e := e_\alpha - e_\beta$
3:	Receive hints $q, r = H_{\text{Div}}(m_\alpha \ll (M+2), m_\beta)$
4:	$C_{\text{RC}}(r, M+1)$
5:	$C_{\text{RC}}(m_\beta - r - 1, M+1)$
6:	$m_\alpha \ll (M+2) = q \cdot m_\beta + r$
7:	$m := q$
8:	$a := a_\alpha \vee C_{\text{IsEq}}(m_\beta, 0)$
9:	Receive hint $b = H_{\text{MSB}}(m)$
10:	$b(1-b) = 1$
11:	$C_{\text{RC}}(m - (b \ll (M+2)), M+2)$
12:	$m := b ? m : m \ll 1$
13:	$e := e + b - 1$
14:	$\Delta e := C_{\text{Max}}(C_{\text{Min}}(-2^{E-1} + 2 - e, M+2, E+1), E+1)$
15:	$e', m' := C_{\text{FPRound}}(e, m, \Delta e, C_{\text{IsEq}}(r, 0))$
16:	$a' := a \vee C_{\text{GEZ}}(e' - 2^{E-1}, E+1)$
17:	$m'_{\text{is}_0} := C_{\text{IsEq}}(m', 0)$
18:	$e' := a' ? 2^{E-1} : ((m'_{\text{is}_0} \vee a_\beta) ? -2^{E-1} + 1 - M : e')$
19:	$m' := a_\beta ? 0 : (a' ? 2^M : m')$
20:	return $s, e', m', a'$

Figure 17: Circuit for floating-point division

$q, r := H_{\text{Div}}(v, 2^d)$  as hints to the circuit. Then to check the predicate  $P_{\text{Div}}(v, 2^d, q, r)$ , it is required to enforce that  $q \in [0, 2^L - 1]$ , i.e.,  $q \cdot 2^d$  does not overflow, that  $r \in [0, 2^d - 1]$ , i.e., the remainder should be positive and smaller than the divisor, and that  $v = q \cdot 2^d + r$ . We can see that checking the range of  $q$  requires decomposing an  $L$ -bit integer, and checking the range of  $r$  requires decomposing two  $K$ -bit integers  $r$  and  $2^d - 1 - r$  (note that the upper bound  $2^d - 1$  is a variable). This is suboptimal, as the above checks are equivalent to decomposing an  $L + 2K$ -bit integer.

We observe that it is possible to reduce the number of bits to be decomposed if, instead of directly computing  $v \gg d$ , the prover first computes  $v' := v \ll (K - d) = v \cdot 2^{K-d}$ . Since  $d \in [0, K]$ , we have  $K - d \in [0, K]$ , and thus  $v \cdot 2^{K-d} < 2^{L+K} < p$  is safe. Then we handle  $v' \gg K$  analogously: the prover computes the quotient  $q$  and the remainder  $r$  for  $v' / 2^K$  and provides  $q, r = H_{\text{Div}}(v', 2^K)$  as hints, and the circuit checks the predicate  $P_{\text{Div}}(v', 2^K, q, r)$  by asserting that  $q \in [0, 2^L - 1]$ ,  $r \in [0, 2^K - 1]$ , and  $v' = q \cdot 2^K + r$ . Another way to understand how to check  $v' \gg K$  is that the circuit first decomposes  $v'$  into  $L + K$  bits, and then computes  $q = \sum_{i=0}^{L-1} 2^i v'_i$ . The optimized approach only requires decomposing  $L + K$  bits, saving  $O(K)$  constraints.

## B CIRCUIT FOR FLOATING-POINT DIVISION

Dividing an IEEE 754 floating-point number  $\alpha = (s_\alpha, e_\alpha, m_\alpha, a_\alpha)$  by another  $\beta = (s_\beta, e_\beta, m_\beta, a_\beta)$  is done in the following 4 steps – (i) computing the quotient of  $\alpha$  and  $\beta$ , (ii) normalizing and (iii) rounding the intermediate mantissa and (iv) handling edge cases. We depict the corresponding in-circuit logic in Figure 17.

**Compute quotient (lines 1-8).** Analogous to multiplication, the sign of the quotient is  $s := s_\alpha \oplus s_\beta$ , the exponent is  $e := e_\alpha - e_\beta$ . However, extra care is needed for computing the mantissa. As per IEEE 754, the intermediate mantissa should have infinite precision, while for division, it is practically infeasible to represent the exact quotient when  $m_\beta \nmid m_\alpha$ . To address this, we instead divide  $\alpha$ 's scaled mantissa  $m_\alpha \ll (M+2)$  by  $m_\beta$  and obtain the quotient  $q$  and remainder  $r$ , such that  $m_\alpha \ll (M+2) = q \cdot m_\beta + r$ , and the intermediate

mantissa is  $m := q$ . Since  $m_\alpha, m_\beta$  are either 0 or lie in  $[2^M, 2^{M+1} - 1]$ , a non-zero, finite  $m$  should be bounded by  $m \in (2^{M+1}, 2^{M+3})$ .

The shift  $M+2$  is the smallest value that allows  $m$  to retain the correct guard bit  $m_{M+1}$ , and  $r$  is used to assist the rounding process and determine the sticky bit, just as if we are rounding a mantissa with infinite precision. This is achieved by checking if  $r$  is zero. If this is the case,  $m_\beta \mid (m_\alpha \ll (M+2))$ , and the remaining bits after the guard bit in the exact result  $\frac{m_\alpha}{m_\beta}$  are all 0, implying that the sticky bit is 0. Otherwise, the sticky bit is 1.

To compute  $(m_\alpha \ll (M+2)) / m_\beta$  inside the circuit, the prover needs to do the division outside the circuit and provide  $q, r := H_{\text{Div}}(m_\alpha \ll (M+2), m_\beta)$  as hints, and the circuit will check the predicate  $P_{\text{Div}}(m_\alpha \ll (M+2), m_\beta, q, r)$  by enforcing (i)  $q \in [0, 2^{2M+3} - 1]$ , (ii)  $r \in [0, m_\beta]$ , and (iii)  $m_\alpha \ll (M+2) = q \cdot m_\beta + r$ . We eliminate the check (i), which is unnecessary as  $q$ 's range will be narrowed to  $[0, 2^{M+3} - 1]$ , as we describe later. (ii) is converted to two range checks since the upper bound  $m_\beta$  is a variable.

The quotient is abnormal if the dividend is abnormal or the divisor is  $\pm 0$  or NaN, i.e.,  $a := a_\alpha \vee C_{\text{IsEq}}(m_\beta, 0)$ .

**Normalize intermediate mantissa (lines 9-13).**  $m$  is normalized in the same way as the normalization of multiplication. Since a non-zero and finite  $m$  is in  $(2^{M+1}, 2^{M+3})$ , the leading 1 of a non-zero  $m$  is either the  $M+1$ -th bit or the  $M+2$ -th bit, and we check if  $m_{M+2} = 1$ . If so,  $m$  and  $e$  are unchanged. Otherwise,  $m := m \ll 1$ ,  $e := e - 1$ , where  $e$  is decremented as  $m_{M+2} = 0$  indicates that the division borrows. The in-circuit operation is similar to normalization for multiplication. The prover feeds  $b := H_{\text{MSB}}(m) = m_{M+2}$ , the MSB of  $m$ , as a hint to circuit, and the circuit checks the predicate  $P_{\text{MSB}}(m, b)$  in 2 steps: (i) enforce  $b$  is a boolean, and (ii) assert  $m - (b \ll (M+2)) \in [0, 2^{M+2}]$ . Note that (ii) implies that  $m \in [0, 2^{M+3} - 1]$ , which indicates the hinted  $m := q$  is the correct quotient mantissa and thus lies in  $(2^{M+1}, 2^{M+3})$ . Finally, the circuit updates  $m, e$  according to  $b$ , i.e.,  $m := b ? m : m \ll 1$ ,  $e := e + b$ .

**Round intermediate mantissa (lines 14-15).** The normalized mantissa  $m$  of length  $N = M + 3$  is rounded as in Section 3.2, with  $\Delta e = \max(\min(-2^{E-1} + 2 - e, K), 0)$ ,  $K = M + 2$ , obtaining  $e'$  and  $m'$ . In addition, the equality between  $r$  and 0 is used to determine the sticky bit, thus we set the in-circuit parameter  $aux := C_{\text{IsEq}}(r, 0)$ .

**Edge Cases (lines 16-20).** Finally, we need to handle the following:

- (i) If the exponent becomes too large, i.e.,  $e' \geq 2^{E-1}$ , then return  $\pm\infty$  (depending on the sign  $s$ ).
- (ii) If the exponent becomes too small, i.e.,  $e' < -2^{E-1} + 1 - M$ , or equivalently, the rounded mantissa becomes 0, then return  $\pm 0$  (depending on the sign  $s$ ).
- (iii) If either  $\alpha$  or  $\beta$  is NaN, then return NaN.
- (iv) If  $\alpha$  is  $\pm\infty$  or  $\beta$  is  $\pm 0$ , then return NaN for  $\pm 0 \div \pm 0$ , and otherwise,  $\pm\infty$  (depending on the sign  $s$ ).
- (v) Otherwise, return  $(s, e', m', 0)$  as the result.

These cases are expressed in-circuit as for multiplication, the only difference is that we return  $\pm 0$ 's exponent and mantissa if  $\beta$  is  $\pm\infty$ . As the result's mantissa is 0 if  $\beta$  is NaN, we use  $a_\beta$  as the condition in  $m' := a_\beta ? 0 : (a' ? 2^M : m')$  to save one boolean operation.



```

CIJK(x, y)
1: a1 := |x|; a2 := |y|
2: x2 :=  $\frac{a_2}{\sin(\frac{\pi}{6})}$ ; x1 := a1 +  $\frac{x_2^2}{2}$ 
3: m1 := ⌊x1⌋; m2 := ⌊x2⌋
4: r1 := x1 - m1; r2 := x2 - m2
5: r1,A = (r1 <  $\frac{1}{2}$ ) ? 1 : 0; r1,A1 = (r1 <  $\frac{1}{3}$ ) ? 1 : 0; r1,B1 = (r1 <  $\frac{2}{3}$ ) ? 1 : 0
6: iA2,1 = (1 - r1 ≤ r2) ? 1 : 0; iA2,2 = (2 · r1 > r2) ? 1 : 0
7: iB1,1 = (r2 > 2 · r1 - 1) ? 1 : 0; iB1,2 = (1 - r1 > r2) ? 1 : 0
8: iA = (iA2,2 ? m1 + 1 : m1); iB = (iB1,1 ? (iB1,2 ? m1 : m1 + 1) : m1 + 1)
9: i = r1,A ? (r1,A1 ? m1 : iA) : (r1,B1 ? iB : m1 + 1)
10: jA = ( $\frac{r_1+1}{2}$  > r2) ? 1 : 0; jB = (1 - r1 > r2) ? 1 : 0; jC = ( $\frac{r_1}{2}$  > r2) ? 1 : 0
11: jA = r1,A1 ? ((jA) ? m2 : m2 + 1) : ((jB) ? m2 : m2 + 1)
12: jB = r1,B1 ? ((jB) ? m2 : m2 + 1) : ((jC) ? m2 : m2 + 1)
13: j = jA ? jA : jB
14: i> = (j < i) ? 1 : 0; i- = (x < 0) ? ((y < 0) ? 1 : i>) : ((y < 0) ? (1 - i>) : 0)
15: iA = (y < 0) ? (i> ? (i - j) : (j - i)) : -i; iB = (i> ? (i - j) : (j - i))
16: i = (x < 0) ? iA : ((y < 0) ? iB : i)
17: return CNormalize(i-, i, y.S, j, 0, 0)

```

**Figure 18: Sub-Circuit for computing the conversion of two dimensional hexagon coordinates  $x, y$  to three dimensional coordinates  $i, j, k$ . Primitive Operations are floating-point as described in Section 3.**

```

CNormalize(i-, i, j-, j, k-, k)
1: i>j = (j < i) ? 1 : 0; i>k = (k < i) ? 1 : 0
2: jA = (j-) ? ((i>j) ? (i - j) : (j - i)) : (i + j); jA- = (j-) ? (1 - i>j) : 0
3: kA = (k-) ? ((i>k) ? (i - k) : (k - i)) : (i + k); kA- = (k-) ? (1 - i>k) : 0
4: i = (i-) ? 0 : i
5: j = (i-) ? jA : j; j- = (i-) ? jA- : j-; k = (i-) ? kA : k; k- = (i-) ? kA- : k-
6: i = (j-) ? (i + j) : i; j = (j-) ? 0 : j; k = (j-) ? kA : k; k- = (j-) ? kA- : k-
7: i = (k-) ? (i + k) : i; j = (k-) ? (j + k) : j; k = (k-) ? 0 : k
8: min = (i>j) ? j : i
9: min = (k < min) ? k : min
10: i = i - min; j = j - min; k = k - min
11: return [i, j, k]

```

**Figure 19: Normalization Sub-Circuit for adjusting  $i, j, k$  coordinates. Primitive Operations are floating-point as described in Section 3.**

## C AUTHENTIC LOCATION INFORMATION

Currently, the ZKLP paradigm described in Section 4 only introduces efficient circuits for transforming  $(\theta, \phi)$  to  $(i, j, k)$  in the Uber H3 [54] hexagonal spatial index. Whilst  $(\theta, \phi)$  are private inputs, and hence not disclosed to the verifier, the prover could still choose arbitrary values as input to the circuit, as it doesn't constrain that location information is obtained correctly, i.e., it does not ensure *data provenance*. We introduce two approaches to mitigate this issue by proving that data comes from a trusted source.

**(i) Authenticated GNSS signals.** Traditionally, GNSS services were designed for military use, and hence the original design did not include robust security features like signal authentication for civilian signals. Further, there is a legacy problem — introducing authentication would require changes to the billions of GPS receivers in use around the world. In recent years, there has been a growing recognition of the security vulnerabilities in GPS, and efforts are being made to enhance its security. Open Service Navigation Message Authentication (OSNMA) is a relatively recent development in GPS technology, aimed at addressing security vulnerabilities, particularly the lack of signal authentication [60], in GPS. There

exist open-source implementations of OSNMA receivers[18], and the underlying cryptographic algorithms are known.

OSNMA uses a combination of ECDSA signatures, the Timed Efficient Stream Loss-tolerant Authentication (TESLA) key chain mechanism, and Messages Authentication Codes (MACs) for message authentication. The receiver's cryptographic operations in OSNMA include verifying a root key of the TESLA chain, authenticating new public keys, verifying TESLA chain keys, and authenticating the MACs of navigation messages. First, the receiver validates the authenticity of a Root Key through an ECDSA signature. Successively, the receiver uses the authenticated root key to verify the current chain key. By successfully verifying the chain key against the root key, the receiver ensures that the chain key is part of the legitimate TESLA key chain. The MAC on the navigation message is a short piece of information generated from the navigation message using a key from the TESLA chain. Using the verified chain key, the receiver then computes the MAC of the navigation data. The computed MAC is compared with the extracted MAC. If they match, it confirms that the navigation message is authentic and has not been tampered with since it was signed.

The TESLA key chain involves a one-way chain of keys, where a random key is utilized as a seed. Computing the chain of keys can be optimized in-circuit through optimizations similar to the ones for Hash functions that are based on the Merkle-Damgard structure [33, 57]. We presume that the overhead of utilizing authenticated GNSS signals with OSNMA will be dominated by the in-circuit verification of ECDSA signatures. Whilst an implementation in gnark exists, at the time of writing, it requires  $4 \cdot 10^6$  constraints for in-circuit emulation over the circuit unfriendly curve secp256k1.

Further, a malicious prover may collaborate with a third party, which obtains the GNSS signal and forwards it. Hence, the verifier needs to ensure that (i) obtaining the location and (ii) computing the proof is conducted *atomically* — which is non-trivial and remains an unsolved problem.

**(ii) TLS Oracles.** Instead of trusting a satellite to provide authentic location information, one may trust a third party entity to verify that location information is obtained from a trusted entity. TLS Oracles [57, 64, 33, 14] provide the possibility to verify data provenance by extending a plain TLS session with a third party, which verifies that the data obtained by a client from a server is authentic. As such, we could extend the ZKLP paradigm to obtain location information from e.g. an API endpoint [22]. The request includes information about nearby cell towers and WiFi access points detected by a mobile client, which can in turn allow for accurate location estimation via an external API.

We leave the details of potential optimizations for authenticated and atomic GNSS, and a concrete system design for integration with TLS oracles, to potential future work.

## D ACCURATE P2P PROXIMITY TESTING

In the following, we describe a more complex method for peer-to-peer proximity testing which more accurate as it accounts for Earth's curvature by converting coordinates into 3D space and then projecting them back. Further, it doesn't check proximity to the vertices of the hexagon, but to the closest point on each line segment between vertices. Let  $\mathcal{H} = \{h_1, h_2, \dots, h_n\}$  be a set of

regular hexagons in the Euclidean plane, where  $\mathbf{h} = [v_0, v_1, \dots, v_i]$  is one such hexagon and each vertex  $v_i = (x_i, y_i)$  is defined in two-dimensional Cartesian coordinates for  $i \in \{0, 5\}$ .  $P_u = (r, \theta, \phi)$  be the position of user  $u$ , where the position on the Earth's surface is given in spatial coordinates by radial distance ( $r$ ), latitude ( $\theta$ ), and longitude ( $\phi$ ). We aim to evaluate the proximity of user  $u$  to user  $v$ , where  $v$  utilizes the previously described protocol to prove that  $P_v \in \mathbf{h}_v$ , such that  $u$  only learns  $\mathbf{h}_v$ . For any two users  $u, v$  the minimal proximity of  $u$  to  $v$  is given by

$$\Delta_{\min}(u, v) = \begin{cases} \min(\delta_1, \delta_2, \delta_3, \delta_4, \delta_5, \delta_6), & \text{if } \mathbf{h}_u \neq \mathbf{h}_v \\ 0, & \text{if } \mathbf{h}_u = \mathbf{h}_v \end{cases}$$

where  $\delta_j =$  distance from  $P_u$  to the  $j$ -th segment of  $\mathbf{h}_u$ .

To evaluate the proximity in plain,  $u$  proceeds by (i) finding the closest point  $P$  on the line segment of  $\mathbf{h}_v$  and (ii) calculating the distance of  $P$  to  $P_u$  on a sphere by utilizing the Haversine formula. First,  $u$  calculates the vertices  $v_i$  for the given  $\mathbf{h}_v$  and converts the geographic coordinates ( $\theta$  and  $\phi$ ) of the vertices  $v_i$  and the point  $P_u$  to the Cartesian coordinate system, i.e.,  $(x, y, z)$  coordinates by utilizing equation 1. Now, we utilize the three-dimensional vectors  $\mathbf{v}_1, \mathbf{v}_2$  and  $\mathbf{L}_u$  in Cartesian  $(x, y, z)$  coordinates to compute the closest point  $P$  on the line segment connecting  $\mathbf{v}_1$  and  $\mathbf{v}_2$  by evaluating the following vector cross products

$$\mathbf{G} = \mathbf{v}_1 \times \mathbf{v}_2,$$

$$\mathbf{F} = \mathbf{L}_u \times \mathbf{G},$$

$$\mathbf{P} = \mathbf{G} \times \mathbf{F}.$$

Successively, we normalize and scale  $\mathbf{P}$  to project it onto the sphere by calculating

$$\mathbf{P}_{\text{norm}} = \frac{\mathbf{P}}{\|\mathbf{P}\|},$$

$$\mathbf{P}_{\text{scaled}} = \mathbf{P}_{\text{norm}} \cdot r.$$

where  $r$  is the radial length of the earth. Successively, we transform  $\mathbf{P}$  in Cartesian coordinates back to spherical geographic coordinates  $P = (\theta_P, \phi_P)$ :

$$\theta_P = \arcsin\left(\frac{z_P}{r}\right),$$

$$\phi_P = \arctan2(y_P, x_P).$$

To calculate the distance between  $P$  and  $P_u$ , we proceed to first convert the coordinates from degrees to radians, as the Haversine formula requires coordinates in radians. The conversion is given by  $\alpha = \text{degrees} \cdot \left(\frac{\pi}{180}\right)$ . Using the Haversine formula,  $u$  can calculate the distance between two points on the Earth's surface. Let  $\theta_1, \phi_1$  and  $\theta_2, \phi_2$  be the latitude and longitude in radians of the two points. The distance  $\delta$  is computed as:

$$a = \sin^2\left(\frac{\theta_2 - \theta_1}{2}\right) + \cos(\theta_1) \cdot \cos(\theta_2) \cdot \sin^2\left(\frac{\phi_2 - \phi_1}{2}\right), \quad (3)$$

$$c = 2 \cdot \arctan2\left(\sqrt{a}, \sqrt{1-a}\right), \quad (4)$$

$$\delta = r \cdot c. \quad (5)$$

The minimum distance  $\Delta_{\min}$  from point  $P_u$  to the boundary of hexagon  $\mathbf{h}$  is the smallest of the distances to each segment of the hexagon:

$$\Delta_{\min} = \min(\delta_0, \delta_1, \delta_2, \delta_3, \delta_4, \delta_5). \quad (6)$$